

Star Formation in the Radio Galaxy NGC 4410A

Megan Donahue¹

*Space Telescope Science Institute, 3700 San Martin Drive, Baltimore, MD 21218,
donahue@stsci.edu*

Beverly J. Smith¹

*East Tennessee State University, Dept. of Physics and Astronomy, Box 70652, Johnson City, TN
37614, beverly@panda.etsu.edu*

and

John T. Stocke¹

University of Colorado, CASA, CB 389, Boulder, CO 80309, stocke@casa.Colorado.edu

ABSTRACT

The NGC 4410 group of galaxies provides us a rare opportunity to study a nearby ($97 h_{75}^{-1}$ Mpc) example of a radio galaxy (NGC 4410A) embedded in an extended X-ray source, with evidence for star formation that can be readily spatially distinguished from regions dominated by the AGN and shocks. We present broadband and narrowband optical images along with optical and IUE ultraviolet spectroscopy for the radio galaxy NGC 4410A and its companion NGC 4410B. Our $H\alpha + [N II]$ images reveal six luminous H II regions ($L_{H\alpha} \sim 10^{40}$ erg s⁻¹) distributed in an arc near NGC 4410A. Partially completing the ring is a prominent stellar loop containing diffuse ionized gas. This filamentary gas, in contrast to the H II regions, shows spectroscopic signatures of shock ionization. The star formation in this system may have been triggered by a collision or interaction between the two galaxies, perhaps by an expanding density wave, as in classical models of ring galaxies. Alternatively, the star formation may have been induced by the impact of a radio jet on the interstellar matter. Extended Ly α is detected in the ultraviolet IUE spectrum. The ultraviolet continuum, which is presumably radiated by the nucleus of NGC 4410A, is not extended. NGC 4410A appears to be interacting with its neighbors in the NGC 4410 group, and could be an example of a spiral galaxy transforming into an elliptical.

Subject headings: galaxies:active, galaxies:interactions, galaxies:individual(NGC 4410A, NGC 4410B), X-rays, infrared radiation, radio continuum, ultraviolet emission, HII regions, quasars:emission lines

¹Visiting Astronomer, Kitt Peak National Observatory

1. INTRODUCTION

We do not understand the link between the radio sources in active galactic nuclei and the emission line regions surrounding those sources. The extended emission line regions around powerful radio galaxies may be radiating light scattered from a central anisotropic source (e.g. Tadhunter et al. 1993; Fabian 1989). Alternatively this gas could be heated by shocks produced by the radio jet interacting with the interstellar medium (ISM), or some combination of shock heating and star formation (Rees 1989; Begelman & Cioffi 1989; De Young 1989). In the centers of cooling flow clusters, the radio galaxy morphology seems to be intimately related to the structures seen radiating optical and near-infrared emission lines typical of star-forming regions or gentle shocks (Donahue et al. 2000; Koekemoer et al. 2000). In the cooling flow clusters, the radio source seems to either excavate a cavity in the emission-line gas or the emission-line gas forms around the radio cavity. Similar structures are seen at high resolution in the latest Chandra images of the central elliptical galaxies in cluster cooling flows such as Hydra A (McNamara et al. 2000). Given the variety of environments of these emission line regions, more than one process may be responsible for the emission-line nebulae in radio galaxies and central galaxies in clusters.

To investigate these issues, we made detailed studies of a nearby radio galaxy in a group of galaxies that is close enough to resolve individual H II regions, the peculiar low-luminosity radio galaxy NGC 4410A. This system is quite nearby ($97 h_{75}^{-1}$ Mpc for $H_0 = 75 h_{75} \text{ km s}^{-1} \text{ Mpc}^{-1}$), and so provides a good target for detailed studies. NGC 4410A, which is classified as an Sab? Pec galaxy on the basis of its optical appearance (de Vaucouleurs et al. 1991), has a prominent bulge surrounded by an extended ring or loop (Hummel, Kotanyi, & van Gorkom 1986). It forms a close pair with the nearby S0? Pec galaxy NGC 4410B. These two galaxies are part of a sparse group containing a dozen known members (Smith 2000). The velocity dispersion of those members is $\sim 220 \pm 70 \text{ km s}^{-1}$, from the velocities reported in Smith (2000), and the group has no obvious group emission (Tschöke et al. 1999). Therefore this group is a poor, X-ray faint group (e.g. Zabludoff & Mulchaey 1998), a classification that is consistent with its lack of elliptical galaxies. The radio luminosity of NGC 4410A is near the faint end of the luminosity range for radio galaxies (Condon, Frayer, & Broderick 1991), with a 4.8 GHz luminosity of $1.5 \times 10^{23} h_{75}^{-2} \text{ W Hz}^{-1}$. The far-infrared (42.5 – 122.5 μm) luminosity of the NGC 4410A+B pair is also moderate, $3.9 \times 10^9 h_{75}^{-2} L_{\odot}$ (Mazzarella, Bothun, & Boroson 1991, calculated as in Lonsdale et al. 1985). The $L_{FIR}/L_{4.8 \text{ GHz}}$ ratio for this system is about 200 times less than expected for a galaxy dominated by star formation, confirming that NGC 4410A contains a radio-loud active nucleus (Condon et al. 1991), in spite of its optical classification as a disk galaxy.

NGC 4410A has a very peculiar radio morphology: a shorter ($3' \sim 80 h_{75}^{-1} \text{ kpc}$) very distorted radio lobe to the southeast (Hummel et al. 1986; Batuski et al. 1992) and a fainter longer structure ($7' \sim 200 h_{75}^{-1} \text{ kpc}$) to the northwest (Smith 2000). This strange radio morphology may have been caused by an interaction of the radio lobe with interstellar matter that has been disturbed by a gravitational encounter between NGC 4410A and NGC 4410B (Smith 2000). NGC 4410A+B contains abundant interstellar matter ($M_{HI} \sim 10^9 h_{75}^{-2} M_{\odot}$ and $M_{H_2} \sim 4 \times 10^9 h_{75}^{-2} M_{\odot}$) (Smith 2000;

assuming the standard Galactic I_{CO}/N_{H_2} conversion factor.) About a third of the HI lies in a tail-like structure extending $1'.7$ ($50h_{75}^{-1}$ kpc) to the southwest, coincident with a faint optical tail (Smith 2000). This tail overlaps with the southeastern radio lobe, suggesting an interaction between the radio jet and the HI gas.

In addition to an active nucleus, NGC 4410A has on-going star formation. In this paper, we present evidence for luminous H II regions in NGC 4410A, in the form of new optical images and optical and ultraviolet spectroscopy.

2. OBSERVATIONS

2.1. Optical Imaging

We observed NGC 4410 on 1989 March 7 using the 512×512 Tek #1 CCD direct camera mounted on the Kitt Peak National Observatory 2.1m telescope. This system provided a pixel size of $0''.34$, giving a field of view of $2'.9$. The seeing was excellent ($\sim 0''.9$) and the sky was photometric. We obtained two 15 minute exposures through an on-band H α filter centered on the redshift of the cluster ($\lambda_o = 6737\text{\AA}$, $\Delta\lambda = 75\text{\AA}$), and a single 15 minute exposure through an off-band filter centered 100\AA blueward ($\lambda_o = 6606\text{\AA}$, $\Delta\lambda = 75\text{\AA}$). The [N II] $\lambda 6548, 6584\text{\AA}$ lines are included in the bandpass of the on-band filter. These images were calibrated by observations of Hiltner 600 made the same night with the same filters and similar air masses. In order to obtain a pure emission-line image of the galaxy, after sky subtraction we used the three brightest stars in the field to derive the ratio of transmission through the on-band and off-band filters. The off-band image was scaled according to this ratio and subtracted from the on-band image.

A larger field of view R-band image of the inner portion of the NGC 4410 group was obtained using the Southeastern Association for Research in Astronomy (SARA) 0.9m telescope on Kitt Peak. These observations were made on 1999 April 18 – 19, using a 2048×2048 Axiom/Apogee CCD. Binning 2×2 , the pixel size is $0''.52$ with this system and the field of view is $8'.9$. The seeing was $\sim 2''$. The total integration time on the galaxy was 40 minutes. Sky flats, darks, and biases were also obtained, and the data were reduced in a standard way.

In this paper, we also discuss an archival Hubble Space Telescope (HST) Wide Field Planetary Camera 2 (WFPC2) image of NGC 4410A², obtained on 1995 April 20. These data consist of a single 500 second exposure taken with the broadband red F606W HST image ($\lambda_0 = 5934\text{\AA}$; $\Delta\lambda = 1498\text{\AA}$). The nucleus of NGC 4410A was centered in the high resolution Planetary Camera (PC) chip of the WFPC2, which provides 800×800 $0''.0455$ pixels. These data were originally obtained

²Based on observations made with the NASA/ESA Hubble Space Telescope, obtained from the data archive at the Space Telescope Science Institute. STScI is operated by the Association of Universities for Research in Astronomy, Inc. under NASA contract NAS 5-26555.

as part of the Malkan, Gorjian, & Tam (1998) HST survey of active galaxies, and have previously been presented by Tschöke et al. (1999) and Smith (2000).

2.2. Optical Spectroscopy

Optical longslit spectra of NGC 4410 were obtained on 1991 December 19 – 20 using the Double Spectrograph mounted at the Cassegrain focus of the Palomar 5m Hale telescope. In the red channel, a 1200 line mm^{-1} grating blazed near 7000\AA was used. This provided a dispersion of 0.817\AA pix^{-1} , a resolution of $\sim 2.5\text{\AA}$, and total wavelength coverage of $6340 - 7000\text{\AA}$. In the blue channel, we used a 300 line mm^{-1} grating, which gave a dispersion of 2.153\AA pix^{-1} , a resolution of $\sim 6\text{\AA}$, and a wavelength range of $3747 - 5250\text{\AA}$.

We made observations at five slit positions in the NGC 4410 system, aligned across the nucleus of NGC 4410A and various knots and features observed in the narrow-band image. Slit positions are indicated in Table 2 and are marked in Figure 1. Individual exposures were 15 minutes in duration. We used a $2''$ slit for all observations. The seeing was $2''$. All observations were conducted at less than 1.1 airmasses.

2.3. Ultraviolet Spectroscopy

Using the International Ultraviolet Explorer (IUE), on 1990 January 30 and February 1 we obtained low-dispersion ultraviolet spectra of NGC 4410 in a $10'' \times 20''$ slit centered on NGC 4410A. The position angle of the slit was 178° east of north. These observations covered a wavelength range of $1150 - 1975\text{\AA}$ with the Short Wavelength Prime (SWP) Camera and $1910 - 3300\text{\AA}$ with the Long Wavelength Prime (LWP) Camera. The SWP exposure was 380 minutes in duration, and the LWP exposure lasted 377 minutes.

3. RESULTS

3.1. The Narrowband Images

The 6606\AA continuum image of NGC 4410A and NGC 4410B is displayed in Figure 2, while the continuum-subtracted $\text{H}\alpha + [\text{N II}]$ map is presented in Figure 3. The ring-like structure of NGC 4410A is evident in both the continuum and the line map. In the continuum map, the western portion of the ring is more prominent, with a bright concentration north of the NGC 4410A nucleus. In the $\text{H}\alpha + [\text{NII}]$ image, a series of unresolved luminous knots lie along the eastern portion of the ring, while an arc of lower surface brightness filamentary emission is visible along the western section of the ring. Both nuclei are detected in $\text{H}\alpha + [\text{N II}]$, and another extremely bright source is visible $5''.4$ southeast of the nucleus. This source is elongated northwest to southeast by $\sim 2''.5$ (1.2

kpc), and is also visible in the continuum image (Figure 2). The nuclei of both galaxies are resolved in the $H\alpha+[N II]$ map, with the center of NGC 4410A being elongated $\sim 10''$ southwest–northeast. In the continuum image, prominent dust features are visible between the two galaxies, near the bright knot southeast of the NGC 4410A nucleus, and south of NGC 4410B.

The total $H\alpha + [N II]$ flux from this system is $3.7 \pm 1.2 \times 10^{-13}$ erg s $^{-1}$ cm $^{-2}$. In Table 1, we provide positions and $H\alpha+[N II]$ fluxes for the centers of the two galaxies and the six brightest knots, along with a total flux for the northwestern arc. These sources are labeled on the $H\alpha+[N II]$ map in Figure 1. The center core of NGC 4410A is six times brighter in $H\alpha+[N II]$ than the center of NGC 4410B, but only 1.8 times more luminous than the most luminous knot, Knot #2. The filamentary arc in the northwest provides $\sim 10\%$ of the total $H\alpha+[N II]$ flux of the system.

Hummel et al. (1986) noted the presence of two optical concentrations in the southeastern tail of NGC 4410A+B. The more northern of these, at $12^h 23^m 58.8^s 9^\circ 16' 14''$ (1950) is in the field of view of our narrowband images. This source was unresolved in the continuum image and was undetected in the $H\alpha+[N II]$ map. The 3σ upper limit to the $H\alpha+[N II]$ flux from this source is 2.9×10^{-16} erg s $^{-1}$ cm $^{-2}$.

3.2. The HST Image

In Figure 4, the ground-based $H\alpha+[N II]$ map is superposed on the archival HST image. We report F606W photometry in Vega magnitudes (m_R) for some of the features inside $0''.96$ apertures. Since good cosmic ray rejection was not possible and the features – most of which are spatially resolved by HST – are embedded in a complex sky background, the photometry is not precise (± 0.2 magnitudes). A good coincidence is found between the knots seen in the narrowband image and clumps in the HST map. In the HST image, these knots are well-resolved. Knot #4 is extended $0''.36 \times 0''.18$ (170×85 pc) east-west, with at least two subknots with $m_r \sim 20.5$ each). Knot #1 is elongated $0''.59 \times 0''.32$ (278×150 pc) northeast to southwest, and has 3 components, with an aperture magnitude of ~ 20.1 . Knot #3 has a larger angular size, $\sim 1''.5 \times 1''.5$ (700 pc \times 700 pc), but a lower surface brightness ($m_R \sim 20$ mag arcsec $^{-2}$, $m_R \sim 21$ in a 0.5 arcsec aperture). The most luminous knot external to the nucleus, Knot #2, is very extended southeast to northwest, with a size of $2''.67 \times 1''.14$ (1.26×0.54 kpc). This knot has three prominent optical peaks and at least six other subclumps. The two brightest subknots ($m_R \sim 18.8$ magnitudes each) in the northeast are separated by $0''.69$ (330 pc), while the third brightest subknot ($m_R \sim 20.7$ magnitudes) lies $1''.14$ (540 pc) to the southeast. These subknots have sizes $\sim 0''.2$ (90 pc).

The dust lanes seen in the groundbased red continuum image are also visible in the HST image and are well-resolved, with widths of $\sim 0''.4 - 1''.4$ ($190 - 660$ pc). These dust features have a patchy filamentary structure, and are visible on both sides of the loop, but are more prominent in the eastern side and surrounding Knot #2. A particularly strong dust lane feature lies just to the southwest of the nucleus, with a position angle of ~ 123 degrees E of N. The dust lane may

obscure the actual nucleus since the peak of the optical emission lies next to the dust lane feature.

3.3. The Ground-Based Broadband Optical Images

In Figure 5, the larger field of view R band image from the SARA telescope is displayed. In this image, five of the galaxies in the inner part of the group are visible: NGC 4410A, B, C, D, and F. The long tail to the southeast of NGC 4410A+B previously noted by Hummel et al. (1986) is evident in this image, as is the broad extension to the northwest of this pair. Roughly calibrating this image using the galaxy magnitudes from de Vaucouleurs et al. (1991) and assuming $B - R \sim 1.5$, we estimate that the two optical knots in the southeastern tail identified by Hummel et al. (1986) have R magnitudes ~ 19 .

3.4. The Optical Spectroscopy

From the long-slit spectra, we extracted $\sim 2'' \times 4''$ aperture measurements for the two nuclei, four of the H II regions, the northwestern arc, and the extended ionized gas east, west, and southwest of the NGC 4410A nucleus. These spectra are displayed in Figure 6. From these data, we extracted line ratios, as well as the central velocity and line width (Table 3). The Galactic extinction in the direction of NGC4410 is very small, with $A_B \sim 0.0$ (Burstein & Heiles 1984), so no intrinsic correction for Galactic absorption was applied to the spectra. The uncertainty in the Galactic absorption introduces up to 0.1-0.05 magnitudes of systemic uncertainty to relative line strengths, particularly for $[\text{O II}]/[\text{O III}]$ and $\text{H}\alpha/\text{H}\beta$. Because the seeing was comparable to the slit width, the absolute photometry is uncertain, so in Table 3 we only provide relative line fluxes and statistical uncertainties. Knot #2 does not have a blue spectrum because it was unresolved from the nucleus in our observations, owing to the poorer optics on the blue side of the Double Spectrograph.

Since the observations were executed at low airmass (< 1.1), the corrections for differential refraction (Filippenko 1982) would be $< 10\%$ for the $[\text{OII}]/\text{H}\beta$ ratios, and $< 2 - 3\%$ for the $\text{H}\alpha/\text{H}\beta$ ratios for the position angles used. One of the observations, Observation 1 with a position angle of 25 degrees, was very close to the parallactic angle of 33 degrees. The differences between the ratios for Knot #1 at this position angle exceed that provided by differential refraction.

When possible, the $\text{H}\alpha/\text{H}\beta$ ratio was used to estimate the extinction to each region (Table 4), assuming an intrinsic $\text{H}\alpha/\text{H}\beta$ ratio of 2.85 (case B) for the H II regions and 3.1 (Ferland & Netzer 1983) for the NGC 4410A nucleus, along with additional, probably conservative, systematic uncertainties of 12% for the line ratios. A dust screen with the extinction curve of Seaton (1979) was assumed. In most cases, the implied extinction is moderate ($A_V \sim 1 - 1.5$). If stellar absorption at $\text{H}\beta$ relative to that at $\text{H}\alpha$ is significant, the actual extinction from dust is somewhat lower. Stellar absorption can remove a few Angstroms of equivalent width from the $\text{H}\beta$ emission line. The typical equivalent width of $\text{H}\beta$ emission was $(-)\text{3-8}\text{\AA}$, so moderate stellar absorption could cause an

overestimate by 0.4-0.8 magnitudes of the absorption at $H\beta$. We note that if the ionized gas and dust are well-mixed, the amount of dust present is higher than what is inferred from extinction derived from assuming a screen.

Comparison of the observed line ratios (Table 3) with standard diagnostic line-ratio diagrams used to distinguish ionization mechanisms (e.g., Baldwin, Phillips, & Terlevich 1985; Veilleux & Osterbrock 1987) confirms that the bright knots of ionized gas are H II regions. In contrast, the nuclei of the two galaxies fall in the Low Ionization Emission Line Region (LINER) regime, consistent with the classification of these galaxies’ nuclear spectra by Mazzarella & Boroson (1993). The $[N II]6584/H\alpha$ ratio is high in both nuclei, and the $[S II]6717/H\alpha$ and $[O I]6300/H\alpha$ ratios are enhanced in the NGC 4410A nucleus. The fainter NGC 4410B nucleus is undetected in $[S II]6717$ and $[O I]6300$. LINER-like spectra are common in radio galaxies (e.g., Baum & Heckman 1989; Baum, Heckman, & van Breugel 1990). The northwestern arc also has enhanced $[N II]6584/H\alpha$, $[S II]6717/H\alpha$, and $[O I]6300/H\alpha$ ratios, indicating that energy input to the gas in this region may be dominated by shocks or other heating mechanisms as opposed to the radiation from hot stars. The extended emission to the southwest, east, and west of the NGC 4410A nucleus has ratios in between those of H II regions and LINER spectra, suggesting that light from both the nucleus and nearby H II regions may have contributed to the extracted spectra.

Additional evidence that we are distinguishing regions dominated by AGN activity from H II regions in NGC4410 comes from the line widths and the lack of strong continuum in the H II sources. The nucleus of NGC 4410A has relatively broad lines (FWHM ~ 600 km s $^{-1}$). The NGC 4410B nucleus and the filamentary features also appear to have somewhat broad lines (FWHM ~ 400 km s $^{-1}$) compared to those of the knots (FWHM $\sim 200 - 300$ km s $^{-1}$), which are only marginally resolved. The knot sources have very little continuum, consistent with their identification as H II regions.

The velocity structure of the ionized gas in this system (Figure 7) is intriguing. The two nuclei, the northwestern filament, and the extended emission to the east of the NGC 4410A nucleus are considerably redshifted (7440 km s $^{-1} - 7500$ km s $^{-1}$) from the H II regions and the extended emission to the southwest and east of the NGC 4410A nucleus, centered at 7130 – 7340 km s $^{-1}$). It is possible that we are viewing line emission from two interacting systems with a velocity separation of ~ 200 km s $^{-1}$, or that the H II regions were originally associated with one of the nuclei.

3.5. The Ultraviolet Spectra

The IUE data were extracted and calibrated by the IUE New Spectral Imaging Processing System (NEWSIPS) software in two ways: the standard extraction method which is optimized for a point source, and a re-extraction and reprocessing using a method optimized for an extended source. The two SWP spectra are plotted in Figure 8.

The 1216Å Ly α feature is strongly detected in this source, with a total line flux of 1.0 ± 0.2

$\times 10^{-13} \text{ erg s}^{-1} \text{ cm}^{-2}$. A possible 1548+1551Å C IV feature may be present at the level of $6 \pm 2 \times 10^{-14} \text{ erg s}^{-1} \text{ cm}^{-2}$, but this feature coincides with the presence of some cosmic rays and the wavelength centroid of the feature places it significantly bluer (by about 400 km sec^{-1}) of the centroid of the Ly α feature, and lies about $4.5''$ south of the position of the continuum source. If real, it may be associated with Knot #2, but we are doubtful.

The mean continuum between 1350-1450 Å observed frame in the SWP spectrum is $1.1 \pm 0.2 \times 10^{-15} \text{ erg s}^{-1} \text{ cm}^{-2} \text{ Å}^{-1}$. The continuum flux from the SWP spectrum obtained with the extended source algorithm is statistically equal to that found with the point source algorithm centered on the continuum peak ($1.2 \pm 0.2 \times 10^{-15} \text{ erg s}^{-1} \text{ cm}^{-2} \text{ Å}^{-1}$), indicating that the continuum emission is unresolved by IUE (FWHM $< 3''.5$). The LWP spectrum (not shown) contains only faint, flat continuum emission, at a mean level of $4 \pm 2 \times 10^{-16} \text{ erg s}^{-1} \text{ cm}^{-2} \text{ Å}^{-1}$ at 3000Å.

Ly α is clearly visible in both extracted spectra, and the flux obtained with the extended source method is higher than that derived assuming a point source. In Figure 8, the amplitude of the Ly α emission line from the extended source extraction ($\sim 1.2 \times 10^{-14} \text{ erg s}^{-1} \text{ cm}^{-2} \text{ Å}^{-1}$) is higher than that obtained from the point-source extraction ($\sim 0.5 \times 10^{-14} \text{ erg s}^{-1} \text{ cm}^{-2} \text{ Å}^{-1}$), indicating that Ly α is extended. The extent of the Ly α emission is $> 20''$, since the emission seems to fill the IUE aperture.

The velocity of the Ly α line is $7050 \pm 50 \text{ km s}^{-1}$. This velocity is inconsistent with the optical velocity of the NGC 4410A nucleus, but similar within the uncertainties with the optical velocities of the H II regions (Table 3), indicating that much of the Ly α emission may originate in the H II regions rather than the nucleus, as expected from the extended spatial distribution of the Ly α emission.

The total observed H α luminosity from the NGC 4410A+B system is $2.2 \times 10^{41} \text{ erg s}^{-1}$, after correction for [N II] using the spectroscopic results in Table 3 and assuming the diffuse emission has line ratios similar to the northwest arc. This gives an overall Ly α /H α flux ratio for this system of ~ 0.50 . The expected intrinsic Ly α /H β ~ 40 from photoionization calculations, but the observed ratio is affected by geometry and resonant scattering effects. Assuming Case B recombination line ratios for H α /H β ~ 2.8 (Osterbrock 1989) and the extinction curve of Seaton (1979), the observed Ly α /H α ratio implies an average extinction $A_V \sim 1.7$ towards the system, somewhat higher than but less reliable (Giavalisco, Koratkar & Calzetti 1996) than the extinctions estimated from the H α /H β ratios (Table 4).

4. DISCUSSION

4.1. Star Formation in NGC 4410

Both star formation and non-thermal nuclear activity are occurring in NGC 4410A, as well as possible shock-ionization of interstellar matter. Here we will discuss the evidence for all of these

phenomena, but in particular for on-going star formation in NGC 4410. We compare the star formation evidence in this peculiar, perhaps intermediate morphological type, galaxy with star formation signatures in other classes of galaxies.

Our $H\alpha+[N II]$ map reveals the presence of both compact knots and diffuse extended emission, as well as extended emission associated with the two nuclei. Our optical spectroscopy indicates that the knots are H II regions, the filamentary structure to the northeast of the nucleus may be shock-ionized, and the nuclei of NGC 4410A and NGC 4410B have LINER spectra. As noted in the Introduction, NGC 4410A has a peculiar double-lobed radio structure (Smith 2000), and a low far-infrared to 4.8 GHz radio luminosity ratio, therefore NGC 4410A contains both a radio-loud active nucleus and on-going star formation.

The H II region complexes in NGC 4410 are very luminous. Knot #2 has $L_{H\alpha} = 3.4 \times 10^{40}$ erg s⁻¹ (corrected for $[N II]6584$ using the $[N II]6584/H\alpha$ ratio in Table 3, but uncorrected for extinction). This is twice as luminous as the ‘supergiant’ H II region 30 Doradus in the Large Magellanic Cloud (Kennicutt 1984). The other H II region complexes in NGC 4410 have $H\alpha$ luminosities ranging from $0.23 - 1.0 \times 10^{40}$ erg s⁻¹. These lie near the top of the H II region luminosity function in nearby spiral and irregular galaxies (Kennicutt, Edgar, & Hodge 1989; Elmegreen & Saltzer 1999). The sizes of the HST subknots associated with these H II regions, ~ 90 pc, are typical of those of OB associations in nearby spiral galaxies (Bresolin, Kennicutt, & Stetson 1996; Bresolin et al. 1998).

We can estimate how much of the emission-line luminosity arises from young stars by separately measuring the total emission excluding the two nuclei and the northwestern arc, which are probably not ionized by young stars, and the emission from the distinct H II regions. Excluding the two nuclei and the northwestern arc, the total observed $L_{H\alpha}$ for NGC 4410 is 1.5×10^{41} erg s⁻¹, uncorrected for internal extinction. The sum of the $H\alpha$ luminosities of the known H II regions in NGC 4410 is 6.5×10^{40} erg s⁻¹. The difference between these two luminosities is due to the extended ionized gas outside of the northwestern arc; it is not yet clear whether this is ionized by young stars or other mechanisms. These two numbers define the range of the $H\alpha$ luminosity provided by OB stars. Applying an extinction correction of $A_V \sim 1.2$ (Table 4) gives $L_{H\alpha}$ from star formation between 1.6×10^{41} erg s⁻¹ and 3.6×10^{41} erg s⁻¹. These $H\alpha$ luminosities are typical for nearby spiral and irregular galaxies (Kennicutt 1983; Young et al. 1996). Using the extended Miller-Scalo initial mass function (Kennicutt 1983), the total star formation rate in NGC 4410 is $1 - 4 M_{\odot} \text{ yr}^{-1}$. This level of star formation relative to the blue luminosity in NGC 4410 is relatively low compared to that in disk galaxies with similarly high blue luminosities. The blue luminosity of NGC 4410A is $5.7 \times 10^{10} L_{\odot}$ (using B_T from de Vaucouleurs et al. 1991 and $M_{B_{\odot}} = 5.48$). The $L_B/L_{H\alpha}$ ratio is $600 - 1700$, at the high end of the range for spiral and irregular galaxies (Young et al. 1996). NGC 4410 is thus not a starburst: its current star formation rate in NGC 4410 is modest compared to its past star formation rate, as inferred from the blue luminosity. NGC 4410A has an absolute blue magnitude of -21.1, approximately that of M87. It is by far the most luminous galaxy in the group, providing 25% of its total blue luminosity (Smith 2000). It may have come by its stellar

content by a high rate of star formation in the past or by stealing stars from other galaxies. The high blue luminosity of NGC 4410A compared to its companions and compared to its current H α luminosity support the hypothesis that it is a spiral turning into an elliptical.

Star formation is probably contributing to the emission line luminosity seen in the nucleus of NGC 4410A in addition to that inferred in the ring. Summing only the flux from the NGC 4410A nucleus and the NW arc, (in the arc, the ionization is probably not due to young stars), $L_{H\alpha+[N+II]}/L_{rad}$ is ~ 7 times higher than the typical value for non-compact, radio-selected radio galaxies. The presence of this excess suggests that even in the central H α + [N II] source of NGC 4410A, young stars may be contributing to the production of H α emission. As noted in §3.4, the spectra of the extended gas east and west of the nucleus have line ratios intermediate between those expected for H II regions and LINERs, suggesting contributions from both classes of processes.

The NGC 4410 far-infrared luminosity of $3.9 \times 10^9 L_{\odot}$ is moderate compared to typical spiral galaxies (e.g. Young et al. 1996). The L_{FIR}/L_B ratio for this system is 0.068, which is in the lower half of the range found for an infrared bright sample of spiral and irregular galaxies studied by Young et al. (1989). Therefore the star formation rate implied by the far-infrared luminosity is only somewhat smaller relative to the blue luminosity compared to infrared-bright galaxies, which are probably forming stars more rapidly than the typical spiral.

Both the far infrared luminosity and the H α luminosity are thought to be good tracers of star formation (e.g. Young et al. 1996). The global $L_{FIR}/L_{H\alpha}$ ratio for NGC 4410, uncorrected for extinction, is 67, somewhat lower than typical for star-forming galaxies (e.g., Devereux & Young 1990; Young et al. 1996). However, using only the observed H α luminosity from young stars gives $L_{FIR}/L_{H\alpha} \sim 100 - 230$, consistent with ratios found for star forming galaxies (Devereux & Young 1990; Young et al. 1996, after correcting for different definitions of far-infrared luminosity). This similarity with star-forming galaxies suggests that massive stars dominate the heating of dust in this system rather than the active nuclei or shocks. It also implies that the H α extinction is not high, consistent with what we find from the optical spectroscopy.

Observations in the 2.6 mm CO (1 – 0) line show that NGC 4410A is rich in molecular gas, with $M_{H_2} = 3.9 \times 10^9 M_{\odot}$ (Smith 2000), assuming the standard Galactic I_{CO}/N_{H_2} conversion factor. Comparing the H α luminosity from young stars to this mass gives $L_{H\alpha}/M_{H_2} = 0.004 - 0.009 L_{\odot}/M_{\odot}$, at the low end of the range for normal spirals and irregulars (Young et al. 1996). Thus NGC 4410 is not forming stars at a particularly high rate compared to the available amount of fuel for star formation, relative to normal spirals. The L_{FIR}/M_{H_2} ratio for NGC 4410A+B is only $\sim 1 L_{\odot}/M_{\odot}$ (Smith 2000), also implying a moderate star formation rate relative to the available molecular gas, at the low end of the range for normal galaxies (Young et al. 1996). At present, CO fluxes of only a handful of radio galaxies have been published to date (Mirabel et al. 1989; Mazzarella et al. 1993; Evans et al. 1999a,b; Lin et al. 2000). Many of these galaxies have L_{FIR}/M_{H_2} ratios higher than that of NGC 4410A+B by a factor of ~ 10 . The Mazzarella et al. (1993) galaxies, however, were selected on the basis of their far-infrared brightnesses, and

have far-infrared luminosities an order of magnitude higher than that of NGC 4410A, so are not an unbiased comparison sample for NGC 4410 in terms of L_{FIR}/M_{H_2} . In the radio-selected survey of Lin et al. (2000), only two of the 19 surveyed radio galaxies were detected above the threshold $\sim 10^8 M_\odot$. Compared to that sample, NGC 4410 has abundant molecular gas.

The CO line width in NGC 4410A is quite broad, with FWHM $\sim 600 \text{ km s}^{-1}$ (Smith 2000). Based on a comparison of the optical and CO velocities (Smith 2000), about 60% of this CO emission may be associated with the H II regions, while the remainder arises from the northwestern filamentary structure. Thus for the eastern and western portions of the ring, $L_{H\alpha}/M_{H_2} \sim 0.007 L_\odot/M_\odot$ and $\sim 0.003 L_\odot/M_\odot$, respectively. The value for the western portion should be considered an upper limit in comparing with values derived for star forming regions, as much of the ionization may be due to shocks rather than young stars.

In contrast, the X-ray emission from NGC 4410 is probably dominated by the AGN and an extended thermal source unrelated to the star formation. The X-ray emission from NGC 4410 in the ROSAT High Resolution Imager (HRI) maps has been resolved into two components: a point source with $L_X = 2.7 \times 10^{41} \text{ erg s}^{-1}$ associated with the nucleus of NGC 4410A, and an extended ($10''$) halo with $L_X = 1.3 \times 10^{41} \text{ erg s}^{-1}$, offset towards Knot #2 (Tschöke et al. 1999). Assuming the halo originates from the star forming regions, it has $L_X/L_{H\alpha} = 2.0$. For the center of NGC 4410A, $L_{H\alpha} = 4.2 \times 10^{40} \text{ erg s}^{-1}$ (Tables 1 and 3), so $L_X/L_{H\alpha} = 6.4$. Pérez-Olea & Colina (1996) find that active nuclei are distinguishable from starbursts by their $L_X/L_{H\alpha}$ ratio: starbursts have $L_X/L_{H\alpha} \leq 0.6$, while active galaxies have higher ratios. The two X-ray components in NGC 4410 both have $L_x/L_{H\alpha}$ ratios higher than the starburst/AGN cutoff, implying that the halo component of the X-ray emission may not be solely due to star formation – a hot ISM, like that found in giant ellipticals, could contribute to the X-ray luminosity.

4.2. Comparison to Other Radio Galaxies

There have been numerous narrowband optical imaging studies of radio galaxies in the past, and the distribution of ionized gas has been mapped in more than 100 radio galaxies (Hansen, Nørggard-Nielsen, & Jørgensen 1987; Baum et al. 1988; Morganti, Ulrich, & Tadhunter 1992; McCarthy, Spinrad, & van Breugel 1995; Hes, Barthel, & Fosbury 1996). In most of these systems, the ionization of the extended gas is believed to be dominated by either photoionization by the active nucleus or shock ionization, rather than young stars (Robinson et al. 1987); such inferences, however, are usually made on the basis of composite spectra. In NGC 4410, $\sim 25\%$ of the total $H\alpha + [N \text{ II}]$ originates from the discrete H II regions, $\sim 60\%$ comes from the two nuclei and the northwestern arc, and 15% is due to diffuse gas outside of these regions. Therefore, even in NGC 4410, young stars do not dominate the ionization. The relative proximity of NGC 4410 to us, however, enables us to spatially resolve structures indistinguishable at higher redshifts, in particular, to separate H II regions from gas ionized by other means. In this section, we compare the global properties of NGC 4410 to those of radio galaxies, and, since we resolve H II regions in NGC

4410A, we discuss what these observations mean for interpretation of emission line regions in radio galaxies.

NGC 4410 appears to have a high emission-line luminosity ($L_{H\alpha+[NII]}$) compared to most radio galaxies. For radio-selected radio galaxies, there is a strong correlation between the $H\alpha+[N II]$ luminosity and the total radio luminosity L_{rad} . This correlation holds not just for high luminosity radio galaxies (Baum & Heckman 1989), but also for low luminosity systems (Morganti, Ulrich & Tadhunter 1992), like NGC4410. Morganti et al. (1992) find a relationship between $L_{H\alpha+[N+II]}$ and L_{rad} for radio sources, excluding compact (size ≤ 10 kpc) radio sources, over five orders of magnitude in radio luminosity. Morganti et al. (1992) find $\log L_{H\alpha+[N+II]} = 0.73 \pm 0.12 \log L_{rad} + 9.93 \pm 4.20$.

The $L_{H\alpha+[N+II]}/L_{rad}$ ratio (but not the linear radio size) of NGC 4410A is similar to the Morganti et al. (1992) compact radio sources. The compact sources in the Morganti et al. (1992) sample have much higher $L_{H\alpha+[N+II]}/L_{rad}$ ratios than the rest of the Morganti sources, up to 20 times higher. Similarly, since NGC 4410A has a total radio luminosity of 1.3×10^{41} erg s⁻¹ (Hummel et al. 1986), $L_{H\alpha}$ for NGC 4410A is 30 times higher than predicted by the Morganti et al. (1992) relation for non-compact radio sources. Morganti et al. (1992) suggest that star formation contributes significantly to the ionization of gas in the compact sources. Star formation contributes significantly in NGC 4410A as well. However, the radio source in NGC 4410A is much larger (280 kpc) than the compact (≤ 10 kpc) radio galaxies in the Morganti et al. (1992) sample.

The far infrared properties of NGC 4410 are consistent with those of a radio galaxy with dust heated by star formation. From the low ratio of far-infrared to radio luminosity (§1), the radio emission is clearly dominated by an active nucleus. However, strong far-infrared emission is not unusual in radio galaxies. In the Golombek, Miley, & Neugebauer (1988) study of 131 radio galaxies, 44% were detected, half with far-infrared luminosities greater than that of NGC 4410. Similar results were found by Impey, Wynn-Williams, & Becklin (1990) for a radio-selected sample. In NGC 4410, as well as in many of the other radio galaxies detected by IRAS, this far-infrared emission is due to interstellar dust, not direct synchrotron radiation from the active nucleus. This is demonstrated for NGC 4410 in Figure 9, where we plot the global spectral energy distribution of NGC 4410A+B. A clear far-infrared excess is seen above the power-law radio continuum. Such an excess is also found in most of the radio galaxies surveyed by Impey et al. (1990). In NGC 4410, the $60 \mu\text{m}/100 \mu\text{m}$ flux density ratio is ~ 0.5 (Mazzarella et al. 1991), within the range found for star forming galaxies (Helou 1986), supporting the idea the far infrared emission could be produced by dust heated by star formation. To distinguish between dust heated by an active nucleus and star formation, the $25 \mu\text{m}/60 \mu\text{m}$ ratio is often used (e.g., de Grijp et al. 1985; Miley, Neugebauer, & Soifer 1985); an enhanced $F_{25 \mu\text{m}}/F_{60 \mu\text{m}}$ ratio signals warmer dust than expect from star formation alone. Based on the IRAS data for NGC 4410, which provides only a 3σ upper limit at $25 \mu\text{m}/60 \mu\text{m}$ of 0.59, we cannot rule out the possibility that emission from hot dust near the active nucleus may contribute to some the far infrared emission.

Whereas the detection of strong far-infrared emission from numerous radio galaxies indicates

that many have reasonably high star formation rates, the direct observations of luminous H II regions in radio galaxies via narrowband optical imaging is still uncommon. One of the few other radio galaxies with H II regions clearly distinguishable in $H\alpha + [N II]$ maps is the peculiar galaxy Centaurus A, which has an inclined dusty disk with numerous H II regions (Hodge & Kennicutt 1983; Bland, Taylor, & Atherton 1987). The far-infrared luminosity of Cen A is $5 \times 10^9 L_{\odot}$ (Rice et al. 1988, using a distance of 3.5 Mpc from Hui et al. (1993)), similar to that of NGC 4410A+B. Most of this far-infrared emission arises from the Cen A disk rather than its nucleus (Joy et al. 1988).

Cygnus A (Stockton, Ridgway, & Lilly 1994; Jackson, Tadhunter, & Sparks 1998) and Hydra A (Melnick, Gopal-Krishna, & Terlevich 1997) also appear to have some circumnuclear star formation, however, the star formation in these systems is much less prominent than that in Cen A or NGC 4410. Fornax A (Mackie & Fabbiano 1998) and PKS 0349-27 (Grimberg, Sadler, & Simkin 1999) show little evidence for the presence of OB stars.

Star formation in a radio galaxy may be triggered by density waves in a disk, as is presumably occurring in the Cen A disk. Alternatively, star formation may be induced by the radio lobe impacting the interstellar medium, which may be the case for Minkowski’s object, a star formation region near the radio galaxy NGC 541 (van Breugel et al. 1985). This object has an $H\alpha$ luminosity of $3 \times 10^{40} \text{ erg s}^{-1}$, similar to that of the most luminous H II region in NGC 4410. Another example of jet-induced star formation may have occurred in 3C 285; like Minkowski’s object, the observed H II region in this system has $L_{H\alpha} = 3 \times 10^{40} \text{ erg s}^{-1}$ (van Breugel & Dey 1993). Jet-induced star formation may also be occurring in Cen A, outside of the main disk. Blue stars and H II regions have been found at the boundary of one of the radio lobes and an HI cloud (Blanco et al. 1975; Graham & Price 1981; Graham 1998). The Cen A H II regions, however, have $H\alpha$ luminosities of only $\sim 3 \times 10^{37} L_{\odot}$, much lower than those found in NGC 4410.

4.3. What Triggered the Star Formation in NGC 4410?

The peculiar star formation morphology of NGC 4410 has several possible origins. Star formation may have been triggered by an expanding density wave, as in classical ring galaxies (e.g., Lynds & Toomre 1976; Theys & Spiegel 1977). The existence of a underlying stellar counterpart to the ring supports this hypothesis; this ring is not solely new stars. The presence of dust on both sides of the ring, in somewhat continuous structures, also supports this idea. If this is indeed a continuous ring, however, it is somewhat distorted. The ring has a position angle of -30° east of north, and an axial ratio of ~ 0.65 (Figures 2 and 4). If this structure is an inherently round ring, the most blueshifted and most redshifted gas would be expected to lie along the major axis. Instead, the line of nodes runs roughly east-west, with the most redshifted gas in the northwestern arc, and the most blueshifted material in Knot #1 (Figure 7).

If the ring was indeed caused by a head-on collision, the most likely collider is NGC 4410B.

The blue luminosity of NGC 4410B is 1/6th that of NGC 4410A (de Vaucouleurs et al. 1991), implying an unequal mass collision. Rings formed by such collisions typically have lifetimes of $\sim 10^8$ years (Theys & Spiegel 1977; Gerber, Lamb, & Balsara 1996), consistent with estimates made for NGC 4410A+B based on pair separation and ring size. Neglecting unknown projection effects, the current separation and velocity difference of the two galactic nuclei, 9.5 kpc and 60 km s⁻¹, imply a time since collision of 1.6×10^8 years. With a projected ring radius of 8'' – 15'' (4 – 7 kpc), assuming an expansion velocity typical of ring galaxies of 50 – 100 km s⁻¹ (e.g., Struck-Marcell & Higdon 1993; Gerber et al. 1996), we estimate a collision timescale of 0.4 – 1.4 $\times 10^8$ years for NGC 4410A, also consistent with theoretical models of ring galaxies.

If NGC 4410A is a classical ring galaxy, however, the observation of line ratios in some of the features consistent with shock ionization may be surprising. The line ratios in ring galaxies are generally typical of H II regions, not shocks (Jeske 1986; Bransford et al. 1998).

Some evidence for an interaction in the group is visible in the X-ray data, in a fainter third X-ray component. In the lower resolution Position Sensitive Proportional Counter (PSPC) map, a faint tail-like structure containing $\sim 10\%$ of the total X-ray flux extends 2' (56 kpc) to the east coincident with the stellar bridge connecting NGC 4410A+B and NGC 4410C (Tschöke et al. 1999; Smith 2000). Such a structure may arise in an interaction between NGC 4410C and its group companions.

Alternatively, star formation may have been triggered by the radio lobe impacting the interstellar medium, as suggested for Minkowski’s object (van Breugel et al. 1985). The fainter radio continuum lobe of NGC 4410 extends to the northwest towards the ring (Smith 2000), however, at present the resolution of the available radio continuum maps is not high enough to determine its spatial association with the H II regions. High resolution radio data would be useful to reveal the answer to this question. The spectroscopic evidence for shocks or at least compressed gas in the northwestern arc, however, supports this alternative hypothesis.

A third possibility is that the ring is the remnant of a third galaxy which has been torn apart by a collision. In this case, Knot #2 may be a third nucleus. The relatively narrow optical line widths of this source (Section 3.4), however, argues against this interpretation.

4.4. The Nature of the Optical Knots in the Southeastern Tail

In the southeastern NGC 4410 lobe, a prominent radio ‘hot spot’ is found, coincident with an optical knot (Hummel et al. 1986). Hummel et al. (1986) suggested that this optical structure may be associated with the radio knot in some manner. It is possible that this source is a ‘hot spot’ emitting optical synchrotron emission, as is believed to be the case for the optical knots studied by Keel & Martini (1995), O’Dea et al. (1999), and Lähteenmäki & Valtaoja (1999). The 4.9 and 1.5 GHz flux densities of the NGC 4410 knot are 2.5 mJy and 4.4 mJy, respectively, with a spectral index α ($F_\nu \propto \nu^\alpha$) of -0.47 . The optical counterpart has an R magnitude of ~ 19 (§3.2), giving

an optical/4.9 GHz spectral index of ~ -0.31 , similar to that in the radio. The estimated index supports the idea that the optical emission is due to synchrotron emission. However, the NGC 4410 knot is unresolved in our narrowband red image (FWHM $\leq 0''.9 \sim 400$ pc), while the radio continuum knot has a size of $\sim 15''$ (7 kpc) (Hummel et al. 1986), arguing against an association. For comparison, the optical hot spots studied by Lähteenmäki & Valtaoja (1999) have linear sizes between 1 and 7 kpc.

Alternatively, this knot may be an H II region, either caused by the interaction or induced by the pressure of the jet impacting the interstellar medium. Evidence for such jet-induced star formation has been found in a number of systems (e.g., de Young 1981; van Breugel et al. 1985; van Breugel & Dey 1993; Graham 1998). This optical knot, however, was not detected in our H α + [N II] map, giving $L_{H\alpha} \leq 3.5 \times 10^{38}$ erg s $^{-1}$. This is lower than the luminosities of the H II regions in the tails of the Antennae galaxy (Mirabel, Dottori, & Lutz 1992) and the Mice pair (Hibbard & van Gorkom 1996), and lower than the luminosity of Minkowski’s object. However, this upper limit is consistent with the H α luminosities of the H II regions in the tails of NGC 2782 (Smith et al. 1999), Arp 295, NGC 520, and NGC 3621 (Hibbard & van Gorkom 1996), as well as the possible jet-induced H II regions in Cen A studied by Graham (1998). Thus, the lack of observed H α emission associated with the northern knot in the NGC 4410 tail does not rule out on-going star formation.

A third possibility is that these knots may be old stellar clusters. If they are at the distance of NGC 4410, they have $M_R \sim -16$, similar to the most luminous of the so-called ‘super star clusters’ found in the inner regions of interacting galaxies by HST (e.g., Holtzman et al. 1992). Finally, these sources could be background or foreground objects. These last possibilities could be resolved with optical colors and/or spectroscopy.

4.5. The NW Arc

The broad H α line and the strong forbidden lines in the NW arc show that it is not ionized by standard H II regions (Section 3.4), particularly evident from the high [OI]6300Å/ H α ratio. Line ratios in this range are typical of AGN (e.g. Veron-Cetty & Veron 2000), cooling flows (Heckman et al. 1989; Voit & Donahue 1995), and gas that has been shock-ionized (e.g. Shull & McKee 1979; Dopita & Sutherland 1996). The cooling flow spectra can be explained by a composite of hot star photoionization and some other source of heat (Voit & Donahue 1995); very slow shocks could contribute, but Voit & Donahue (1995) and Donahue et al. (2000) argue that such shocks are very inefficient at producing H α . Extended emission to one side of the nucleus could be produced by the asymmetric production of radiation from the AGN, as in the cone structures observed in Seyferts (e.g. Capetti et al. 1994; Wilson et al. 1989). The emission is similar to the line emission produced by collisional debris as seen in NGC 4438, a spiral galaxy which has apparently recently interacted with a companion S0 galaxy (Kenney et al. 1995). Extensive plasma diagnostics to sort out the various possibilities are not possible with the spectrum in hand, lacking the detection of

[OIII] and other fainter diagnostic lines.

Based on the ROSAT X-ray image of this system, we can rule out a cooling flow as the dominant source of heat for the NW arc. The thermal X-ray emission from the NGC 4410A+B vicinity is $\leq 1.3 \times 10^{41} h_{75}^{-2} \text{ erg s}^{-1}$ (Tschöke et al. 1999); this value is only an upper limit to the luminosity arising from cooling flow gas, since some of the X-ray radiation must originate from X-ray binaries in the star formation regions (Section 4.1). For comparison, the $H\alpha$ luminosity of the NW arc is $2 \times 10^{40} h_{75}^{-2} \text{ erg s}^{-1}$ (Tables 1 and 3). Therefore $L_{H\alpha}/L_X \geq 0.15$, much higher than typical cooling flow clusters, where $L_{H\alpha}/L_X$ is less than 0.02, even when the X-ray luminosity from the cooling flow is computed in a region local to the optical filaments (Heckman et al. 1989).

In other radio galaxies, there have been numerous observations of extended ionized gas exterior to the nuclear regions. As discussed in §4.2, in some cases, H II regions have been found in other radio galaxies. In most cases, however, the extended ionized gas found in other radio galaxies has line ratios consistent with shock ionization (Robinson et al. 1987), similar to those found in the NW arc of NGC 4410.

5. Conclusions

NGC 4410A is the host of both a radio-loud active nucleus and on-going star formation. The star formation is in the form of extremely luminous H II regions aligned in an arc along the eastern portion of a ring-like stellar structure surrounding the active nucleus. The western portion of this ring contains filamentary ionized gas with optical line ratios implying shock ionization. NGC 4410A is thus a nearby example of an AGN with spatially-resolved evidence for both star formation and shocks in an extended emission line region. Such an object lends credence to the hypothesis that the emission line regions associated with radio galaxies and the central galaxies in cluster cooling flows might also result from the effects of more than one phenomenon, with the implication that no single physical process can explain all of the observations. NGC 4410A could be an example of a disk galaxy on its way to becoming an elliptical, via interactions with its group companions.

We thank James Webb for help with the SARA observations. We are grateful to Cathy Imhoff (MAST) for assistance with the NEWSIPS package and discussions regarding the IUE data. This research has made use of the NASA/IPAC Extragalactic Database (NED) which is operated by the Jet Propulsion Laboratory under contract with NASA. Some of the data presented in this paper were obtained from the Multimission Archive at the Space Telescope Science Institute (MAST). STScI is operated by the Association for Universities for Research in Astronomy, Inc. under NASA contract NAS5-26555. Support for MAST for non-HST data is provided by the NASA Office of Space Science via grant NAG5-7584 and by other grants and contracts. We would also like to acknowledge the use of the Double Spectrograph at the Palomar Observatory (5-meter), then under joint support by the Observatories of the Carnegie Institution of Washington and the

California Institute of Technology. We also obtained data from facilities at the Kitt Peak National Observatory, which is funded by the National Science Foundation and operated by the Association of Universities for Research in Astronomy, Inc. B. J. S. acknowledges support from NASA grant AR-08374.01-97A from the Space Telescope Science Institute.

REFERENCES

- Baldwin, J. A., Phillips, M. M., & Terlevich, R. 1981, *PASP*, 93, 5.
- Batuski, D. J., Hanisch, R. J., & Burns, J. O. 1992, *AJ*, 103, 1077.
- Baum, S. A., Heckman, T., Bridle, A., van Breugel, W., & Miley, G. 1988, *ApJS*, 68, 643.
- Baum, S. A., & Heckman, T. 1989, *ApJ*, 336, 681.
- Baum, S. A., Heckman, T., & van Breugel, W. 1990, *ApJS*, 74, 389.
- Begelman, M. C. & Cioffi, D. F. 1989, *ApJ*, 345, L21.
- Blanco, V. M., Graham, J. A., Lasker, B. M., & Osmer, P. S. 1975, *ApJ*, 198, L63.
- Bland, J., Taylor, K., & Atherton, P. D. 1987, *MNRAS*, 228, 595.
- Bransford, M. A., Appleton, P. N., Marston, A. P., & Charmandaris, V. 1998, *AJ*, 116, 2757.
- Bresolin, F., Kennicutt, R. C., Jr., & Stetson, P. B. 1996, *AJ*, 112, 1009.
- Bresolin, F., et al. 1998, *AJ*, 116, 119.
- Burstein, D. & Heiles, C. 1984, *ApJS*, 54, 33.
- Capetti, A., Macchetto, F., Sparks, W. B. 1994, *ApJ*, 421, 87.
- Condon, J. J., Frayer, D. T., & Broderick, J. J. 1991, *AJ*, 101, 362.
- de Grijp, M. H. K., Miley, G. K., Lub, J. & de Jong, T. 1985, *Nature*, 314, 240.
- de Vaucouleurs, G., de Vaucouleurs, A., Corwin, Jr., H. G., Buta, R. J., Paturel, G., & Fouque, P. 1991, *Third Reference Catalogue of Bright Galaxies, Version 3.9 (RC3)*.
- Devereux, N. A., & Young, J. S. 1990, *ApJ*, 350, L25.
- de Young, D. S. 1981, *Nature*, 293, 43.
- de Young, D. S. 1989, *ApJ*, 342, L59.
- Donahue, M., et al. 2000, *ApJ*, 545, 670.
- Dopita, M. A. & Sutherland, R. S. 1996, *ApJS*, 102, 161.
- Elmegreen, D. M., & Salzer, J. J. 1999, *ApJ*, 117, 764.
- Evans, A. S., Kim, D. C., Mazzarella, J. M., Scoville, N. Z., & Sanders, D. B. 1999a, *ApJ*, 521, L107.
- Evans, A. S., Sanders, D. B., Surace, J. A., & Mazzarella, J. M. 1999b, *ApJ*, 511, 730.

- Fabian, A. C. 1989, MNRAS, 238, P41.
- Ferland, G. & Netzer, H. 1983, ApJ, 264, 105.
- Filippenko, A. V. 1982, PASP, 94, 715.
- Gerber, R. A., Lamb, S. A., & Balsara, D. S. 1996, MNRAS, 278, 345
- Giavalisco, M., Koratkar, A., & Calzetti, D. 1996, ApJ, 466, 831.
- Golombek, D., Miley, G. K., & Neugebauer, G. 1988, AJ, 95, 26.
- Graham, J. A. 1998, ApJ, 502, 245.
- Graham, J. A., & Price, R. M. 1981, ApJ, 247, 813.
- Grimberg, B. I., Sadler, E. M., & Simkin, S. M. 1999, ApJ, 521, 121.
- Hansen, L., Nørgaard-Nielsen, H. U., & Jørgensen, H. E. 1987, A&AS, 71, 465.
- Heckman, T. M., Baum, S., van Breugel, W. J. M., & McCarthy, P. 1989, ApJ, 338, 48.
- Helou, G. 1986, ApJ, 311, L33.
- Hes, R., Barthel, P. D., & Fosbury, R. A. E. 1996, A&A, 313, 423.
- Hibbard, J. and van Gorkom, J. 1996, AJ, 111, 655.
- Hodge, P. W., & Kennicutt, R. C. Jr. ApJ, 88, 296.
- Holtzman, J. A., et al. 1992, AJ, 103, 691.
- Hui, X., Ford, H. C., Ciardullo, R., & Jacoby, G. H. 1993, ApJ, 414, 463.
- Hummel, E., Kotanyi, C. G., & van Gorkom, J. H. 1986, A&A, 155, 161.
- Impey, C. D., Wynn-Williams, C. G., & Becklin, E. E. 1990, ApJ, 356, 62.
- Jackson, N., Tadhunter, C., & Sparks, W. B. 1998, MNRAS, 301, 131.
- Jeske, N. A. 1986, Ph. D. Thesis, University of California at Berkeley.
- Joy, M., Lester, D. F., Harvey, P. M., & Ellis, H. B. 1988, ApJ, 326, 662.
- Keel, W. C. & Martini, P. 1995, AJ, 109, 2305.
- Kenney, J. D., Rubin, V. C., Planesas, P., & Young, J. S. 1995, ApJ, 438, 135.
- Kennicutt, R. C., Jr. 1983, ApJ, 272, 54.
- Kennicutt, R. C., Jr. 1984, ApJ, 287, 116.
- Kennicutt, R. C., Jr., Edgar, B. K., & Hodge, P. W. 1989, ApJ, 337, 761.
- Koekemoer, A. M. et al. 2000, ApJ, 525, 621.
- Lähteenmäki, A. & Valtaoja, E. 1999, AJ, 117, 1168.
- Lin, J., Leon, S., Combes, F. & Trung, D. V. 2000, ApJ, 545, L93.
- Lonsdale, C. J., Helou, G., Good, J. C., & Rice, W. 1985, Catalogued Galaxies and Quasars Observed in the IRAS Survey (Pasadena: Jet Propulsion Laboratory).

- Lynds, R., & Toomre, A. 1976, *ApJ*, 209, 382.
- Mackie, G., & Fabbiano, G. 1998, *ApJ*, 115, 514.
- Malkan, M. A., Gorjian, V., & Tam R. 1998, *ApJS*, 117, 25.
- Mazzarella, J. M., Bothun, G. D., & Boroson, T. A. 1991, *AJ*, 101, 2034.
- Mazzarella, J. M. & Boroson, T. A. 1993, *ApJS*, 85, 27.
- Mazzarella, J. M., Graham, J. R., Sanders, D. B., & Djorgovski, S. 1993, *ApJ*, 409, 170.
- McCarthy, P. J., Spinrad, H., & van Breugel, W. 1995, *ApJS*, 99, 27.
- McNamara, B. R. et al. 2000, *ApJ*, 534, L135.
- Melnick, J., Gopal-Krishna, & Terlevich, R. 1997, *A&A*, 318, 337.
- Miley, G. K., Neugebauer, G., & Soifer, B., 1985, *ApJ*, 293, L11.
- Mirabel, I. F., Sanders, D. B., & Kazèz, I. 1989, *ApJ*, 340, L9.
- Mirabel, I. F., Dottori, H., Lutz, D. 1992, *A&A*, 256, L19.
- Morganti, R., Ulrich, M.-H., & Tadhunter, C. N. 1992, *MNRAS*, 254, 546.
- O’Dea, C. P., de Vries, W., Biretta, J. A., & Baum, S. A. 1999, *AJ*, 117, 1143.
- Osterbrock, D. E. 1989, “Astrophysics of Gaseous Nebulae and Active Galactic Nuclei,” (University Science Books: Mill Valley, CA).
- Pérez-Olea, D. E. & Colina, L. 1996, *ApJ*, 468, 191.
- Rees, M., 1989, *MNRAS*, 239, P1.
- Rice, W., Lonsdale, C. J., Soifer, B. T., Neugebauer, G., Koplan, E. L., Lloyd, L. A., de Jong, T., Habing, H. J. 1988, *ApJS*, 68, 91.
- Robinson, A., Binette, L., Fosbury, R. A. E., & Tadhunter, C. N. 1987, *MNRAS*, 227, 97.
- Seaton, M. J. 1979, *MNRAS*, 187, 73p.
- Shull, J. M. & McKee, C. S. 1979, *ApJ*, 227, 131.
- Smith, B. J., Struck, C., Kenney, J. D. P., & Jogee, S. 1999, *AJ*, 117, 1237.
- Smith, B. J. 2000, *ApJ*, 541, 624.
- Stockton, A., Ridgway, S. E., & Lilly, S. J. 1994, *AJ*, 108, 414.
- Struck-Marcell, C., & Higdon, J. L. 1993, *ApJ*, 411, 108
- Tadhunter, C. N., Scarrott, S. M., Draper, P., & Rolph, C. 1993, *MNRAS*, 256, P53.
- Theys, J. C., & Spiegel, E. A. 1977, *ApJ*, 212, 616
- Tschöke, D., Hensler, G., & Junkes, N. 1999, *A&A*, 343, 373.
- van Breugel, W., Filippenko, A. V., Heckman, T., & Miley, G. 1985, *ApJ*, 293, 83.
- van Breugel, W. J. M. & Dey, A. 1993, *ApJ*, 414, 563.

- Veilleux, S. & Osterbrock, D. E. 1987, *ApJS*, 63, 295.
- Véron-Cetty, M. P. & Véron, P. 2000, *Astronomy & Astrophysics Review*, 10, 81.
- Voit, G. M. & Donahue, M. 1995, *ApJ*, 452, 164.
- Wilson, A. S., Wu, X. N., Heckman, T. M., Baldwin, J. A., & Balick, B. 1989, *ApJ*, 339, 729.
- Young, J. S., Xie, S., Kenney, J. D. P., & Rice, W. L. 1989, *ApJS*, 70, 699.
- Young, J. S., Allen, L., Kenney, J. D. P., Lesser, A., & Rownd, B. 1996, *AJ*, 112, 1903.
- Zabludoff, A. I. & Mulchaey, J. S. 1998, *ApJ*, 496, 39.

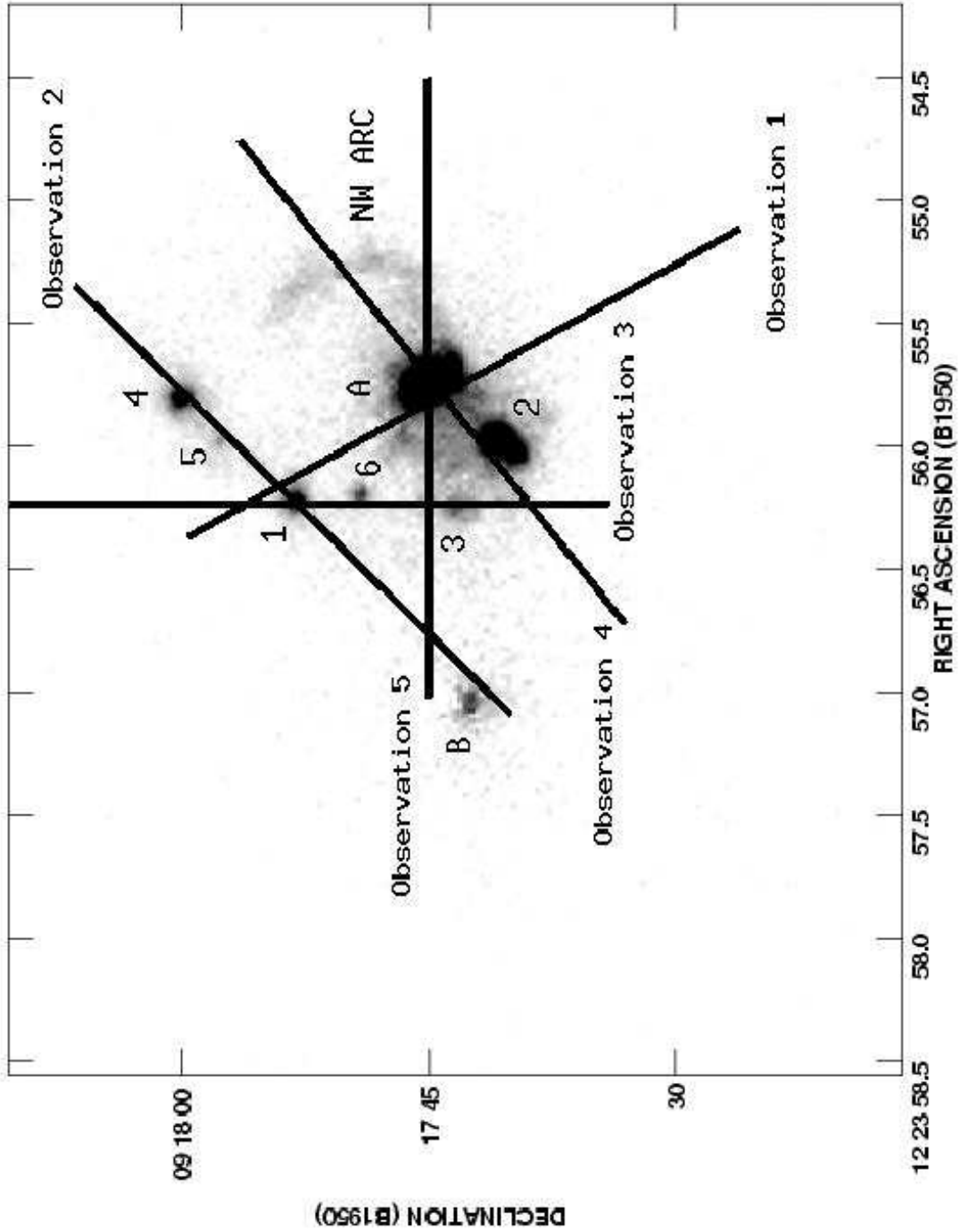


Fig. 1.— The locations of the slit positions on NGC 4410 for the optical spectroscopy, superposed on the $H\alpha + [N II]$ image. The actual slit widths were $2''$ wide; the accuracy of the slit locations is about $0.5-1.0''$, based on telescope slew offsets from a nearby star. Features like Knot #2 and nucleus B were probably not well-centered in the slit. The H II regions tabulated in Table 1 are identified in this figure.

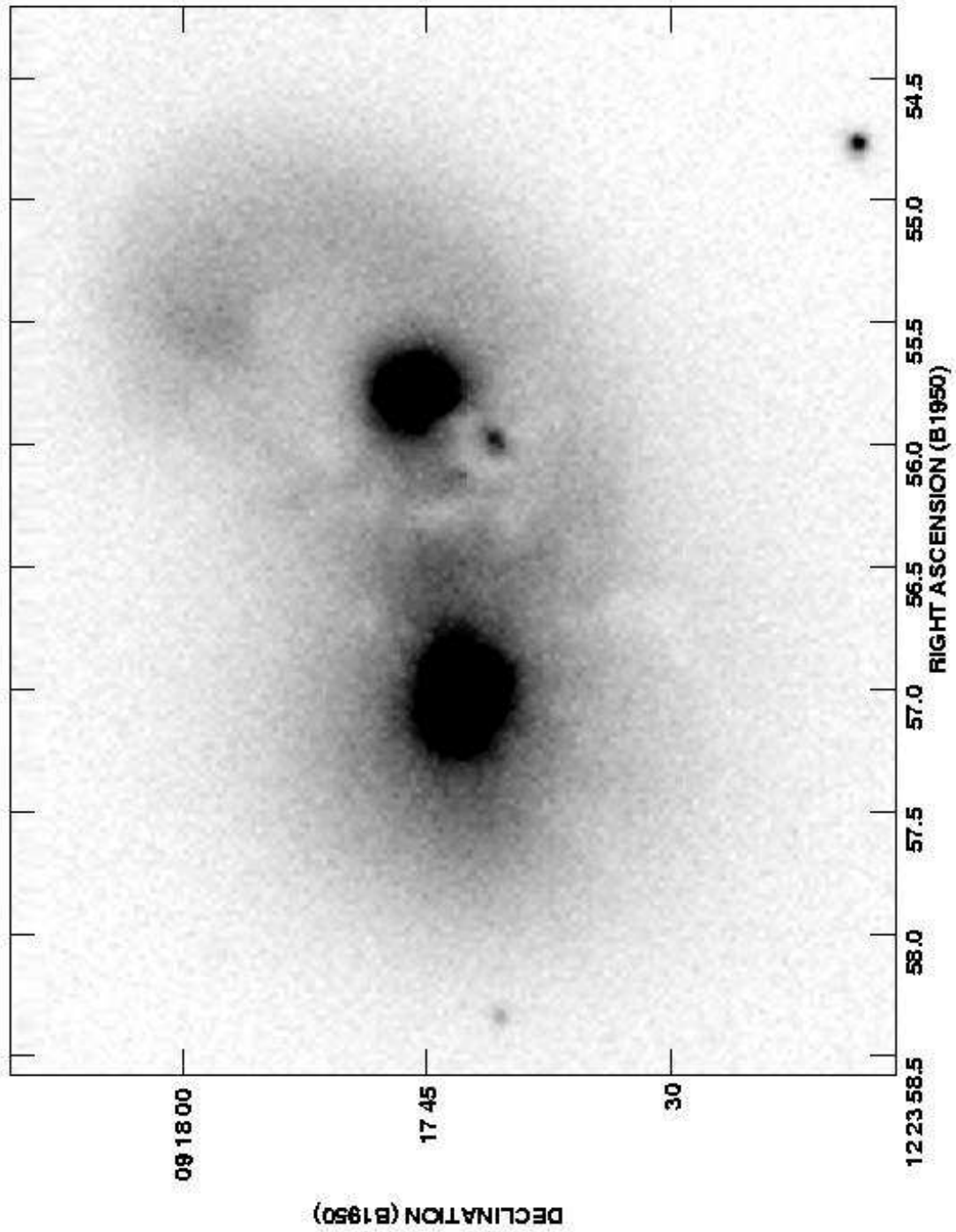


Fig. 2.— The inner $65'' \times 54''$ of the narrowband 6606\AA continuum image of NGC 4410A (to the west) and NGC 4410B. Note the ring-like structure to the northwest of NGC 4410A and the bright knot $5''.4$ southeast of the nucleus of NGC 4410A.

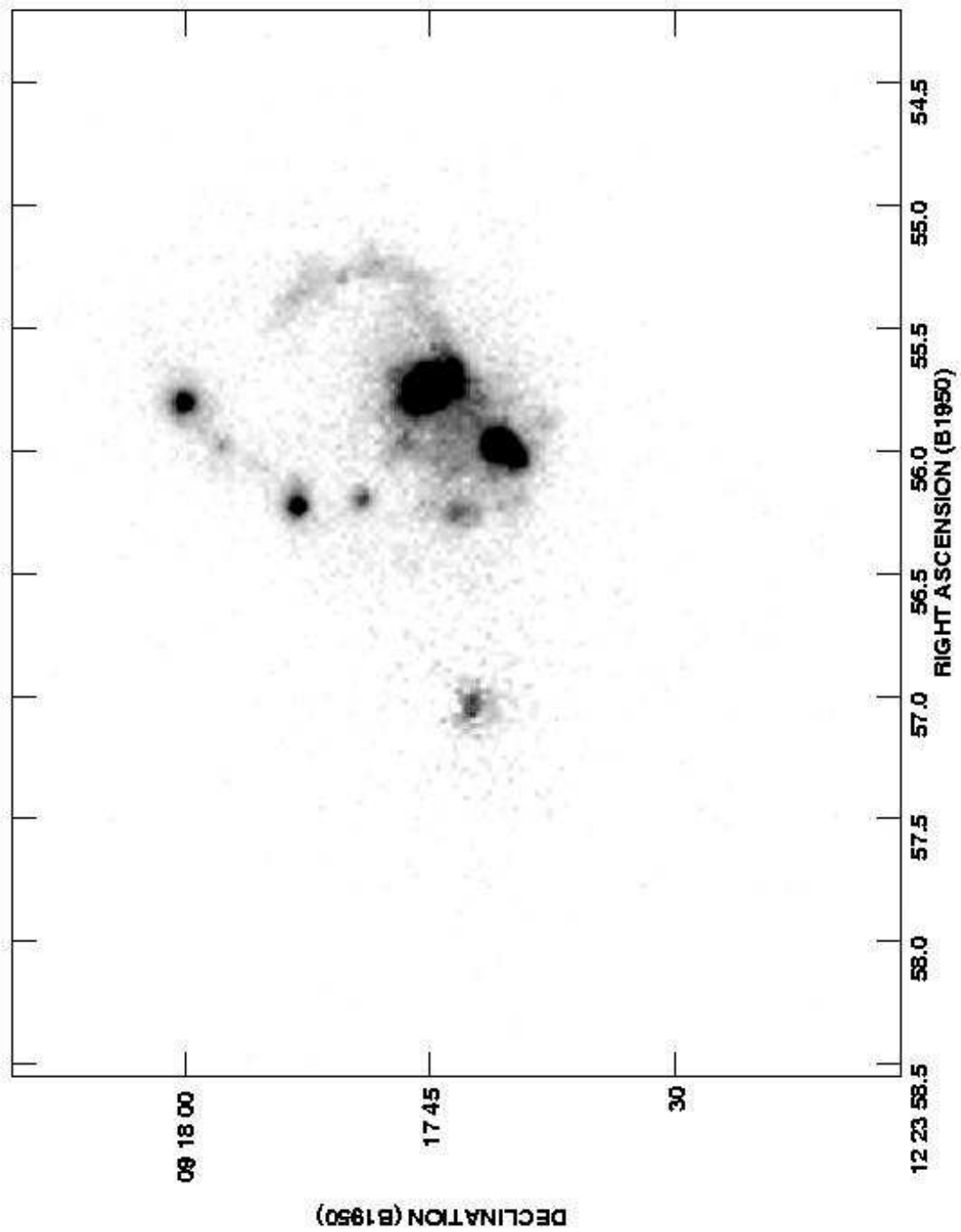


Fig. 3.— The inner 65'' \times 54'' of the continuum-subtracted H α + [N II] image of NGC 4410A and NGC 4410B. Both galactic nuclei are visible in this image, as well as the luminous knot southeast of the NGC 4410A nucleus, a string of five H II regions along the eastern portion of the ring, and a filamentary structure along the western section of the ring.

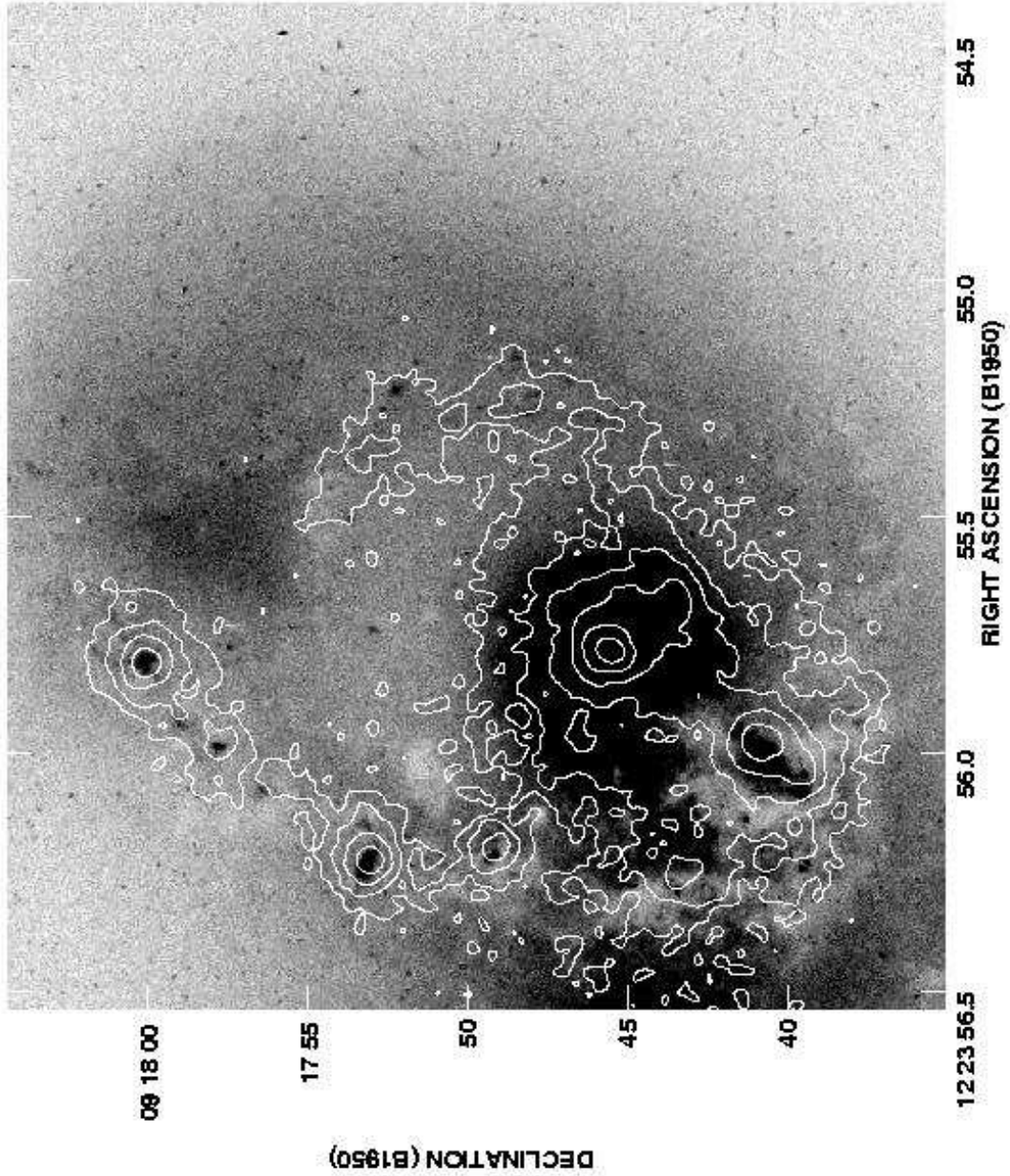


Fig. 4.— The $H\alpha$ + $[N\ II]$ image of NGC 4410 superposed on the HST broadband image. The first contour is 4.1×10^{-16} erg s $^{-1}$ cm $^{-2}$. The contours are logarithmic, increasing by $\Delta \log F = 0.3$.

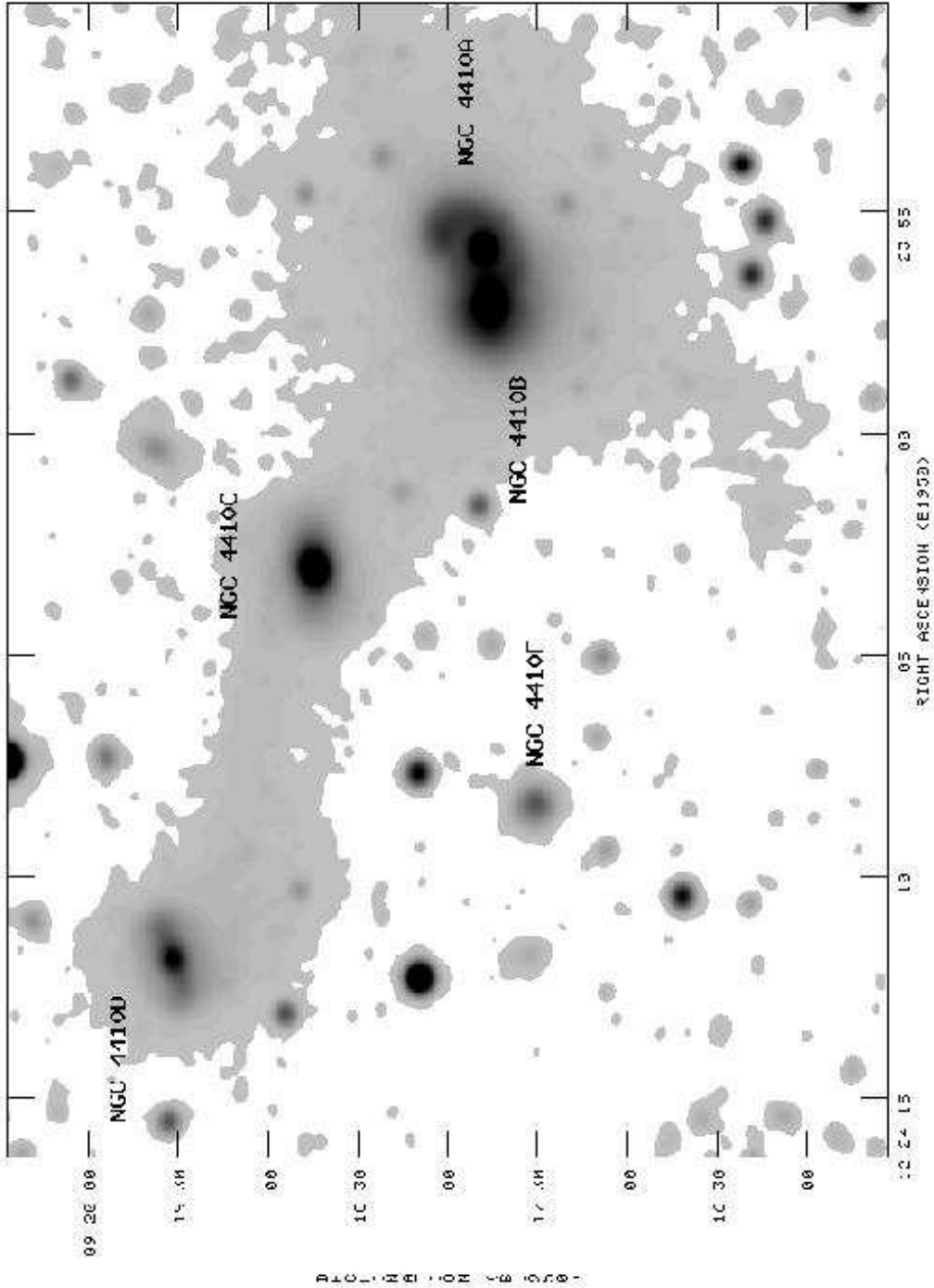


Fig. 5.— The SARA R band image of NGC 4410. The five galaxies in the inner part of the NGC 4410 group are labeled. This image has been smoothed with a 5'' Gaussian to emphasize the faint features. NGC 4410A, B, and C are classified as Sab? Pec, S0? Pec, and S0? respectively, by de Vaucouleurs et al. (1991). NGC 4410D is classified as SBa(s) by the NASA Extragalactic Database (NED) and NGC 4410E is classified as Sab, Smith (2000).

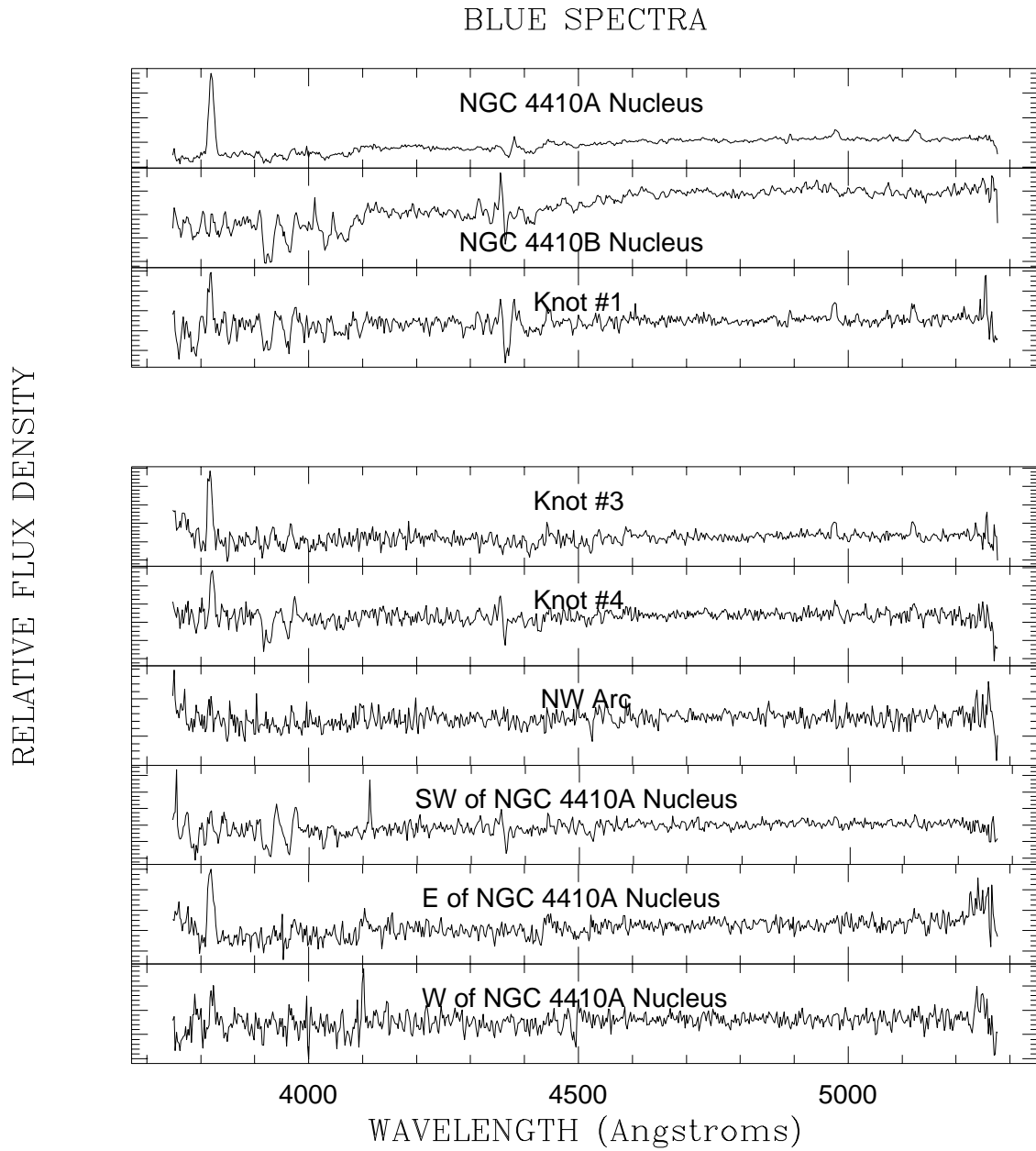


Fig. 6.— A: The blue optical spectra for the 10 selected positions in NGC 4410.

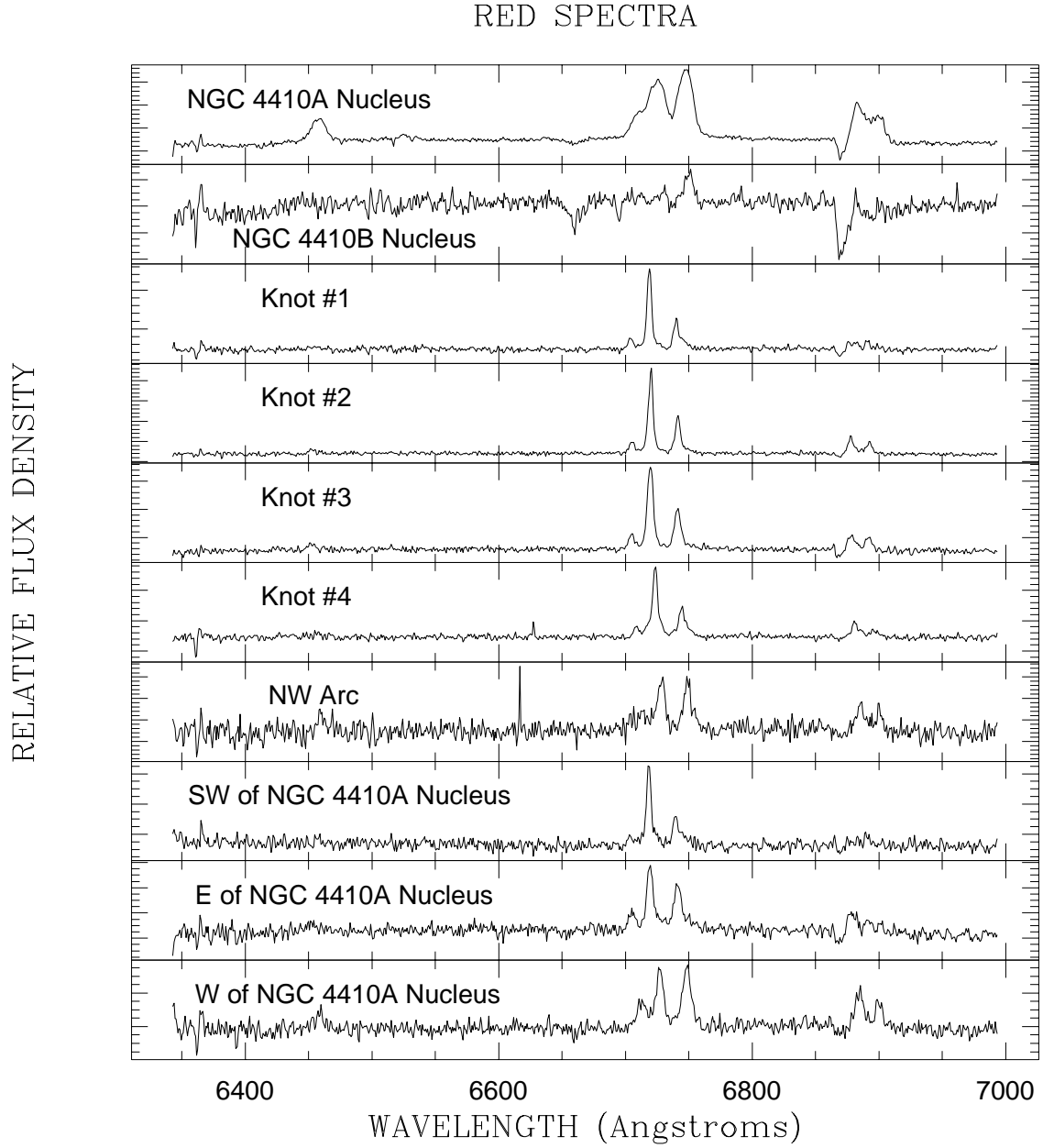


Fig. 6.— B: The red spectra. Multiple observations have been averaged. In the blue spectrum from Observation #4, because of the poorer camera optics on the blue side of the Double Spectrograph, Knot #2 was spatially unresolved from the nucleus. Therefore we do not provide a blue spectrum for this source.

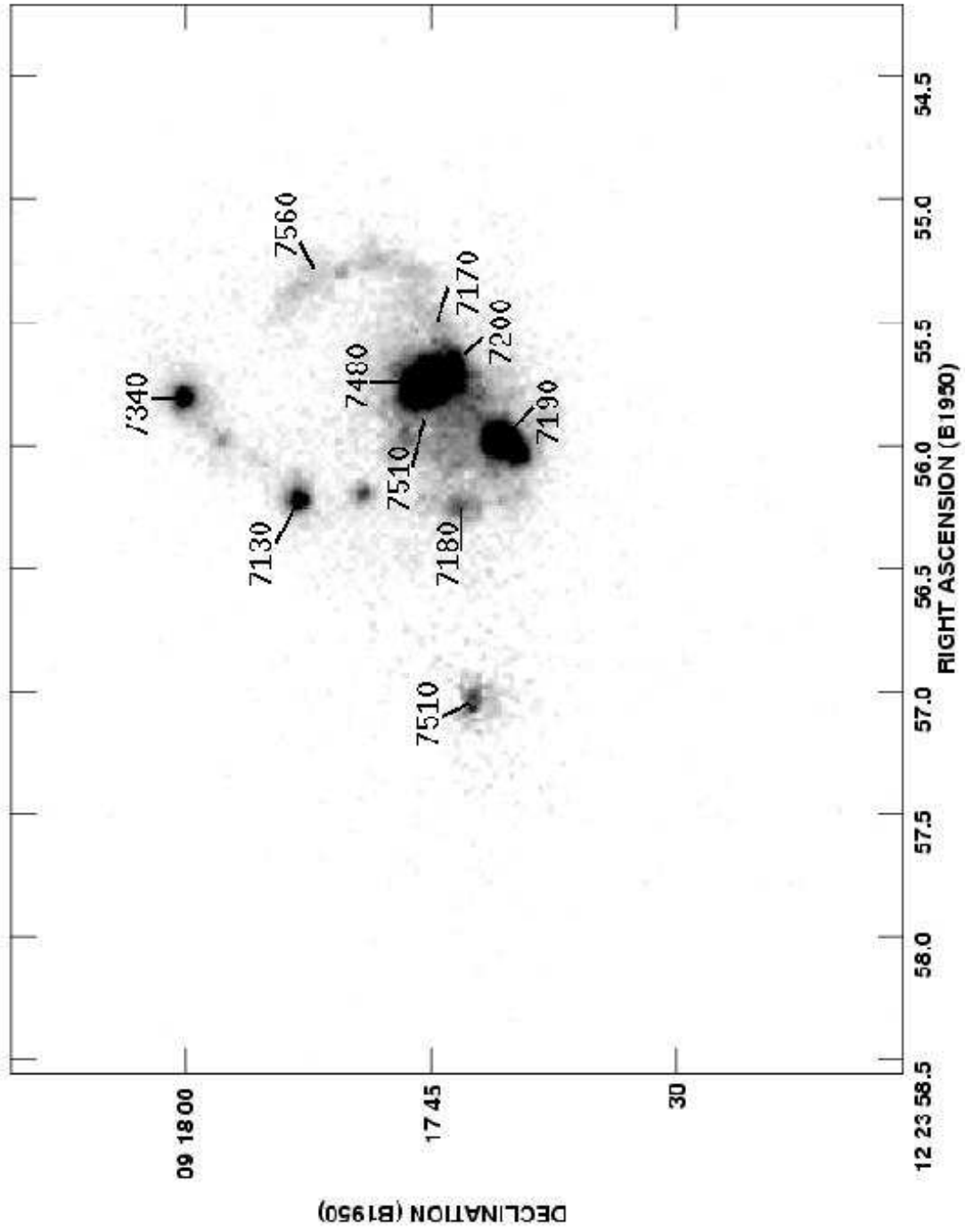


Fig. 7.— The optical velocities marked on the $H\alpha+[N II]$ image.

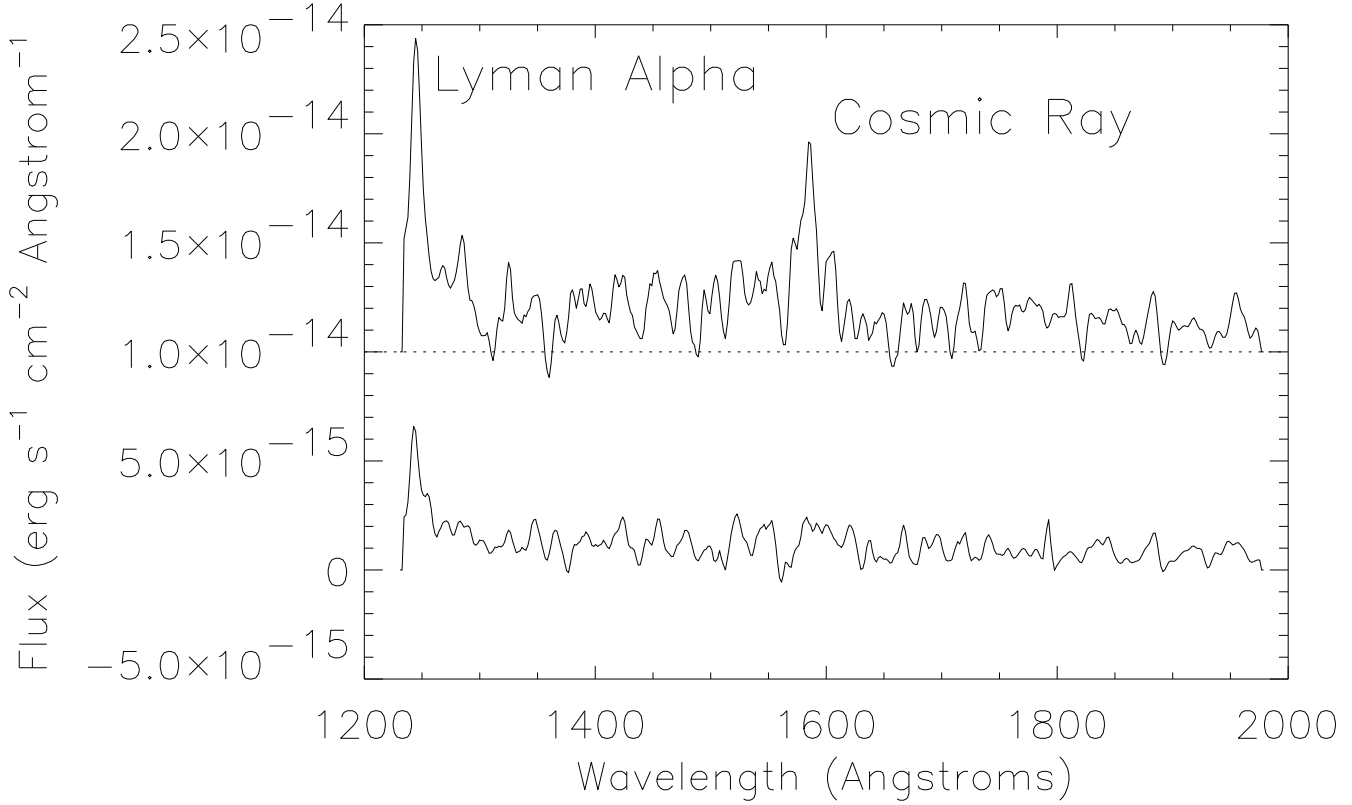


Fig. 8.— The smoothed IUE SWP spectra for NGC 4410A. The top spectrum was obtained by reprocessing the data with the extended source software in NEWSIPS. The lower spectrum was extracted using the standard NEWSIPS point source algorithm. The y-axis is flux, in $\text{erg s}^{-1} \text{cm}^{-2} \text{\AA}^{-1}$ units. For display purposes, the upper spectra has been offset by $10^{-14} \text{erg s}^{-1} \text{cm}^{-2} \text{\AA}^{-1}$, marked as a baseline on the figure. The variations in the continuum are at the level of the noise. The only detected feature is the Lyman- α emission line in both the extended spectrum and the point-source spectrum. The feature near 1570\AA in the extended source spectrum was visually identified as a cosmic ray hit.

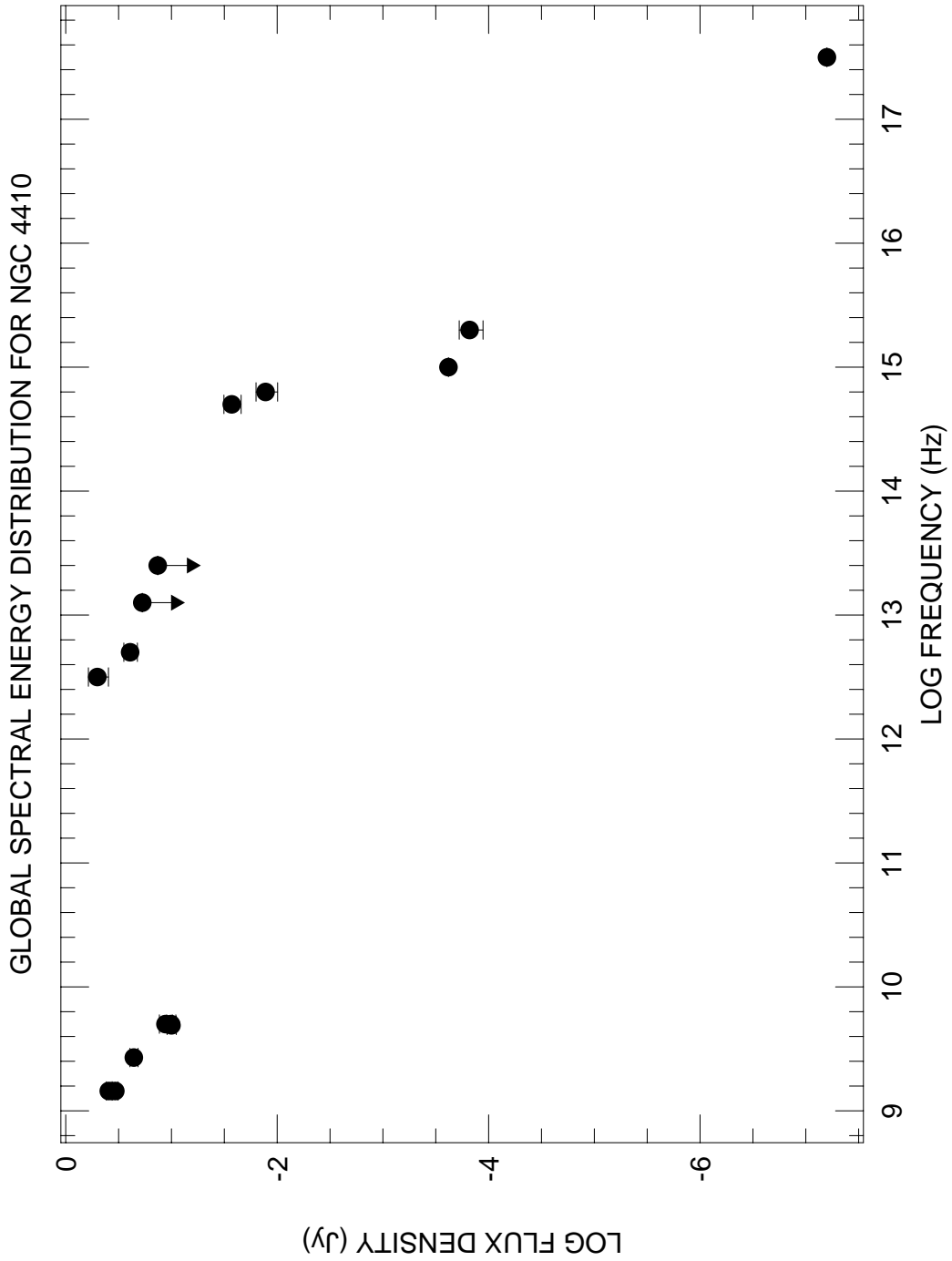


Fig. 9.— The global spectral energy distribution for NGC 4410. The radio data are from Hummel et al. (1986), the far-infrared from Mazzarella et al. (1991), the optical measurements from de Vaucouleurs et al. (1991), the ultraviolet data from this work, and the X-ray points from Tschöke et al. (1999).

Table 1: Nuclei and H II Regions in the NGC 4410A+B System

Name	Position						$L_{H\alpha+[N II]}^a$ (erg s ⁻¹)	Velocity ^b (km s ⁻¹)
	R.A. (1950)		Dec. (1950)					
NGC 4410A Nucleus	12	23	55.78	9	17	45	9.0×10^{40}	7440
NGC 4410B Nucleus	12	23	57.03	9	17	43	1.5×10^{40}	7500
Knot #1	12	23	56.24	9	17	53	1.2×10^{40}	7140
Knot #2	12	23	55.96	9	17	41	5.0×10^{40}	7150
Knot #3	12	23	56.26	9	17	43	8.8×10^{39}	7140
Knot #4	12	23	55.81	9	18	0	1.5×10^{40}	7300
Knot #5	12	23	55.99	9	17	58	3.5×10^{39}	
Knot #6	12	23	56.19	9	17	49	6.1×10^{39}	
NW Arc							3.8×10^{40}	7490

^aAll luminosities were derived assuming a distance of 97 Mpc ($H_0 = 75 \text{ km s}^{-1} \text{ Mpc}^{-1}$). No corrections for internal extinction were applied.

^bHeliocentric velocity from the optical spectroscopy presented in this paper. The uncertainty on these values is $\sim 100 \text{ km s}^{-1}$.

Table 2: Slit Positions for Optical Spectroscopy

Observation	Center Position of Slit	Position Angle	Additional Objects Observed
Observation 1	NGC 4410A Nucleus	25°	Knot #1, Emission SW of A
Observation 2	Knot #1	135°	NGC 4410B Nucleus, Knot #4
Observation 3	Knot #1	0°	Knot #3
Observation 4	NGC 4410A Nucleus	310°	Knot #2, NW Arc
Observation 5	NGC 4410A Nucleus	270°	Emission E and W of A

Table 3: Optical Line Ratios^a

ID/obs	Obs ^b	$\frac{[N II]6584}{H\alpha}$	$\frac{[S II]6717}{H\alpha}$	$\frac{[S II]6717}{[S II]6731}$	$\frac{[O I]6300}{H\alpha}$	$\frac{[O III]5007_{c,d}}{[O II]3727}$	$\frac{H\alpha_d}{H\beta}$	$\frac{[O III]5007}{H\beta}$
N4410A	1	0.97±0.01	0.44±0.01	1.37±0.09	0.28±0.01	0.16±0.01	2.90±0.09	0.98±0.04
	4	1.23±0.01	0.56±0.01	1.38±0.05	0.39±0.01	0.15±0.01	4.20±0.13	1.45±0.05
	5	1.19±0.01	0.51±0.01	1.27±0.05	0.39±0.01	0.13±0.01	5.00±0.17	1.35±0.06
N4410B	2	2.83±0.63	≤0.50	---	≤0.50	---	---	---
Knot #1	1	0.39±0.06	0.07±0.06	0.58±1.56	0.06±0.06	1.24±0.19	1.57±0.18	1.00±0.13
	2	0.51±0.05	0.11±0.05	1.99±2.87	0.14±0.05	0.37±0.04	2.39±0.30	1.26±0.18
	3	0.37±0.02	0.18±0.02	1.62±0.45	≤0.04	0.17±0.02	3.55±0.21	0.57±0.07
Knot #2 ^c	4	0.47±0.02	0.25±0.02	1.32±0.23	0.07±0.02	---	---	---
Knot #3	3	0.50±0.01	0.20±0.01	1.11±0.13	0.09±0.01	0.16±0.01	5.13±0.22	0.92±0.06
Knot #4	2	0.47±0.02	0.25±0.02	1.85±0.51	0.04±0.02	0.23±0.03	6.55±0.94	1.00±0.20
NW Arc	4	0.97±0.10	0.48±0.08	1.38±0.58	0.27±0.07	---	---	---
SW of A	1	0.66±0.05	0.32±0.04	1.25±0.45	0.20±0.04	---	6.80±1.88	1.22±0.43
E of A	5	0.77±0.05	0.33±0.04	2.05±0.85	0.16±0.04	≤0.04	≥10	---
W of A	5	1.09±0.07	0.63±0.06	1.46±0.34	0.29±0.05	---	---	---

^aThese line ratios are uncorrected for extinction and stellar absorption. Note that the dispersions in the line ratios for the three different observations of the NGC 4410A nucleus and Knot #A are larger than the statistical uncertainties, probably because of slight positional offsets.

^bObservation number. See Figure 1 and Table 2.

^cAn artifact on the CCD chip made measurement of the [O II]3727 line impossible in some cases. In the blue spectrum from Observation #4, Knot #2 was spatially unresolved from the nucleus, so we do not provide blue line ratios for this source.

^dThe line ratios of [O III]/[O II] and H α /H β for observations 2-5 (but not Observation 1) would be decreased by 6-10% and 2-3% respectively by the correction for differential refraction.

Table 4: Estimates of Extinction^a

ID/obs		A_V
N4410A	1	-0.16 ± 0.3
	4	0.9 ± 0.3
	5	1.3 ± 0.1
N4410B	2	– – –
Knot #1	1	-1.5 ± 0.3
	2	-0.5 ± 0.5
	3	0.6 ± 0.15
Knot #2	4	– – –
Knot #3	3	1.6 ± 0.2
Knot #4	2	2.3 ± 0.5
NW Arc	4	– – –
SW of A	1	2.5 ± 1.0
E of A	5	≥ 3.5
W of A	5	– – –

^aA systematic uncertainty of 12% in the $H\alpha/H\beta$ ratios was included in the error budget to account for uncertainties in the Galactic extinction (10%) and the smaller uncertainty (2%) in relative slit losses due to differential refraction. No correction for stellar absorption has been applied.